Available online at www.sciencedirect.com
ScienceDirect
Coordination Chemistry Reviews 250 (2006) 2234–2260
COORDINATION CHEMISTRY REVIEWS
www.elsevier.com/locate/ccr

Review

Supramolecular coordination networks based on octacyanometalates: From structure to function

Paweł Przychodzeń, Tomasz Korzeniak, Robert Podgajny, Barbara Sieklucka *

Faculty of Chemistry, Jagiellonian University, Ingardena 3, 30-060 Kraków, Poland

Received 30 August 2005; accepted 26 January 2006
Available online 24 March 2006

Contents

Abstract

The formation of supramolecular assemblies based on octacyanometalates $[M(CN)_8]^{3-/4-}$ (M = Mo, W and Nb) of potential relevance in nanotechnological applications is currently attracting considerable attention. Intensive research in this field resulted in the synthesis and magnetochemical characterization of high-spin polynuclear molecules as well as extended multidimensional coordination networks which behave like molecular or photoinduced magnets. This article discusses the structural and magnetic aspects of the polynuclear systems built by the non-rigid octacyanometalate anionic precursors, from zero-dimensional clusters to three-dimensional frameworks.

Keywords: Molecular materials; Crystal engineering; Octacyanometalates; Magnetic coupling; Photomagnetism; Cyano bridge; Crystal structures

Abbreviations: acacen, *N*,*N*′-ethylenebis(acetylacetonylideneaminato) dianion; AF, antiferromagnetic; ax, axial; 2,2′-bpy, 2,2′-bipyridyl; 4,4′-bpy, 4,4′-bipyridyl; bpym, 2,2′-bipyrimidine; BTP-8, bicapped trigonal prism; 3-CNpy, 3-cyanopyridine; 4-CNpy, 4-cyanopyridine; CTTS, charge transfer to solvent; cyclam, 1,4,8,11-tetraazacyclotetradecane; 0D, zero-dimensional; 1D, one-dimensional; 2D, two-dimensional; 3D, three-dimensional; DD-8, dodecahedron; dien, bis(2-aminoethyl)amine; DMF, *N*,*N*-dimethylformamide; en, 1,2-diaminoethane; eq, equatorial; EtOH, ethanol; F, ferromagnetic; FCM, field-cooled magnetization; H_3Tea, triethanoloamine; IPCT, ion-pair charge transfer; L^1, 2,12-dimethyl-3,7,11,17-tetraazabicyclo[11.3.1]heptadeca-1(17),2,11,13,15-pentaene; L^2, 3,7-bis(2-aminoethyl)-1,3,5,7-tetraazabicyclo[3.3.2]decane; L^3, 2,13-dimethyl-3,6,9,12,18-pentaazabicyclo[12.3.1]octadeca-1(18),2,12,14,16-pentaene; LF, ligand-field; LMCT, ligand-to-metal charge transfer; MeOH, methanol; MSAPR-9, monocapped square antiprism; OC-6, octahedron; 3-OMesalophen, *N*,*N*′-phenylenebis(3-metoxysalicylideneaminato) dianion; OS MMCT, outer-sphere metal-to-metal charge transfer; MMCT, metal-to-metal charge transfer; PBPY-7, pentagonal bipyramid; pn, 1,2-diaminopropane; pym, pyrimidine; salen, *N*,*N*′-ethylenebis(salicylideneaminato) dianion; SAPR-8, square antiprism; SP-4, square planar; SPY-5, square pyramid; T-4, tetrahedron; TBPY-5, trigonal bipyramid; terpy, 2,2′:6′,2″-terpyridine; tetren, 1,11-diamino-3,6,9-triazaundecane; tn, 1,3-diaminopropane; tren, tris(2-aminoethyl)amine; TTP-9, tricapped trigonal prism; ZFCM, zero-field-cooled magnetization

* Corresponding author. Tel.: +48 12 6632036; fax: +48 12 6340515.
E-mail address: siekluck@chemia.uj.edu.pl (B. Sieklucka).

0010-8545/$ – see front matter © 2006 Elsevier B.V. All rights reserved.
doi:10.1016/j.ccr.2006.01.026

1. Introduction

The history of octacyanometalates began in 1904, when Chilesotti obtained the octacyano complex, $K_4[Mo(CN)_8]\cdot 2H_2O$ [1] for the first time. Since then, further studies have led to the synthesis of a series of octacyanometalates $[M(CN)_8]^{3-/4-}$ (M = Mo, W, Nb) and the exhaustive characterization of their reactivity and photochemistry [2–5].

The phenomenon of molecular magnetism and photomagnetism displayed by Prussian blue and its analogues has been widely investigated since the beginning of the nineties [6]. The design and synthesis of new multifunctional molecular magnetic materials was further developed by the use of octacyanometalates in the construction of multidimensional coordination networks since 1995. The research resulted in the synthesis, structural and magnetic characterization of polynuclear high-spin clusters, *spin-flop* molecules, magnetic and photomagnetic coordination networks [7]. The exploration of various cationic 3d-metal precursors resulted in different topologies of the polynuclear octacyano-based coordination networks and different magnetic exchange pathways. However, until 2003 the construction of such networks was limited to assembling d-electron metal centres. The recent use of 4f ions with d-electron octacyano-tectons has opened up new perspectives in the construction and crystal engineering of multifunctional coordination networks. Moreover, the photomagnetic effects displayed by several octacyanometalate-based systems form a potential basis for their applications in data storage, quantum computing or non-linear optics as molecular materials combining magnetic and optical properties.

The main aim of this review is to present the different coordination networks built by $[M(CN)_8]^{3-/4-}$ anionic precursors and discuss the magnetostructural correlations from the viewpoint of a synthetic coordination chemist.

2. Background

2.1. Octacyanometalates: synthesis and photoreactivity

The original synthesis of octacyanometalates of molybdenum and tungsten reported by Chilesotti [1] and Olsson [3] is known to be inefficient with a very complicated purification procedure. Today, the commonly used synthetic method leading to $K_4[Mo(CN)_8]\cdot 2H_2O$ and $K_4[W(CN)_8]\cdot 2H_2O$ is the reduction of sodium molybdate or tungstate by BH_4^- ions in the presence of potassium cyanide and acetic acid [8]. The overall reaction can be described as follows:

$$4MO_4^{2-} + 32CN^- + BH_4^- + 25H^+ \rightarrow 4[M(CN)_8]^{4-} + 13H_2O + H_3BO_3$$

where M = Mo or W. The $[M(CN)_8]^{4-}$ ions can be easily oxidised to $[M(CN)_8]^{3-}$ with concentrated nitric acid [9], sodium nitrite in acidic solution [10] or potassium permanganate or cerium(IV) salts in acidic medium [11].

The photoreactivity of octacyanometalates was discovered early after the first synthesis of $K_4[Mo(CN)_8]\cdot 2H_2O$ [1–4].

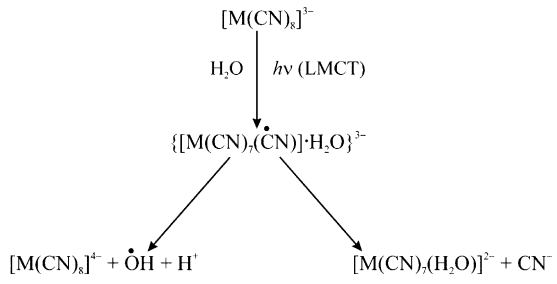

$$[M(CN)_8]^{3-} + [M(CN)_7(H_2O)]^{2-} + 3H_2O \rightarrow [M(CN)_8]^{4-} + MO_4^{2-} + 7CN^- + 8H^+$$

$$8[M(CN)_8]^{3-} + 8CN^- \rightarrow 8[M(CN)_8]^{4-} + 8\dot{C}N$$

Scheme 1.

$$[M(CN)_8]^{4-} \xrightarrow{h\nu\ (CTTS)} *[M(CN)_8]^{4-} \longrightarrow [M(CN)_8]^{3-} + e^-_{solv}$$

Scheme 2.

Systematic studies of the photosubstitution and photoredox processes of $[M(CN)_8]^{3-/4-}$ ions performed until the beginning of nineties resulted in the determination of mechanisms of the photoreactions and identification of photoproducts.

Irradiation of $[M(CN)_8]^{3-}$ system in the lowest energy LMCT band causes the formation of $[M(CN)_8]^{4-}$ ions (Scheme 1) [12].

The photoprocess leading to $[M(CN)_8]^{4-}$ occurs through two parallel pathways: (i) a photoredox reaction giving directly the $[M(CN)_8]^{4-}$ species as a photoproduct, or (ii) photosubstitution giving the $[M(CN)_7(H_2O)]^{2-}$ primary photoproduct which is followed by a series of thermal secondary redox reactions. The quantum yield of the photoredox process was found to be significantly higher ($\Phi_r = 0.8$) than that of the photosubstitution reaction ($\Phi_s = 0.2$).

The photoreaction of $[M(CN)_8]^{4-}$ occurring under CTTS excitation provides the formation of $[M(CN)_8]^{3-}$ and release of the solvated electron (Scheme 2) [13].

On the other hand, irradiation in the LF band opens the pH-dependent substitutional photochemistry of $[M(CN)_8]^{4-}$ ions (Scheme 3) [5(c)].

The photolysis in alkaline medium leads to the formation of $[MO(OH)(CN)_4]^{3-}$ from $[M(CN)_7(OH)]^{4-}$ passing through several intermediates with a variable number of CN ligands. The photoprocess occurring in acidic solution yields a group of

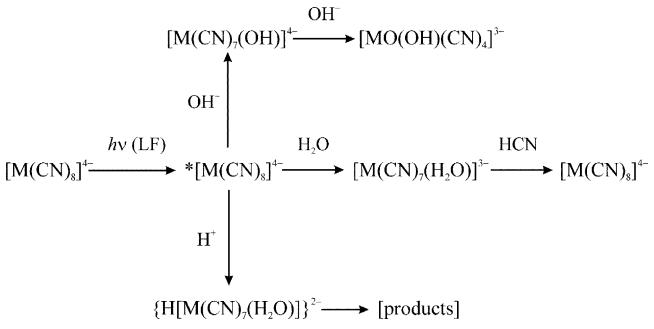

Scheme 3.

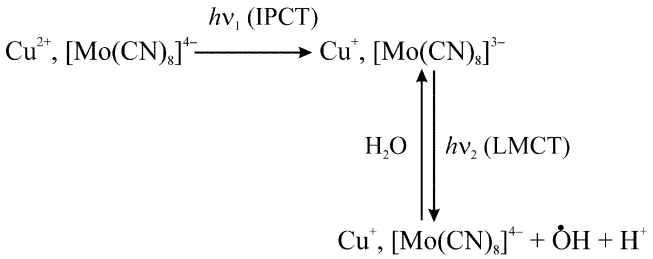

Scheme 4.

products with a different number of CN ligands formed from the protonated $\{H[M(CN)_7(H_2O)]\}^{2-}$ complex.

The formation of mixed-valence ion-pairs characterised by the presence of an ion-pair charge transfer (IPCT) transition in the visible part of electronic spectrum of $[M(CN)_8]^{4-}$ ions formed the basis of their metal-to-metal charge transfer photochemistry in ion pairs with d-electron metal cations (Scheme 4) [14].

Excitation within the IPCT band causes electron transfer and the formation of $[M(CN)_8]^{3-}$ species followed by the photoreduction of octacyanometalate(V) entities after irradiation within its LMCT band.

2.2. Crystal engineering of $[M(CN)_8]^{3-/4-}$-based coordination networks

The design and construction of multidimensional extended systems based on octacyanometalates comprises the exploring of various cationic precursor complexes of 3d- and 4f-electron metal ions as well as two different oxidation states of octacyanometalate anionic precursor. Substitution of labile coordination sites at the cationic building block leads to the formation of cyano-bridged coordination networks from zero- to three-dimensional systems. The use of multidentate blocking ligands at cationic metal centres lowers the dimensionality of the coordination network by limiting the number of possible substitution sites. The self-assembly of cationic complexes of different geometries and different coordination numbers into a cyano-bridged network is accompanied by the stereochemical non-rigidity of $[M(CN)_8]^{n-}$ building block. This results in the octacyanometalate ion adopting one of three limiting spacial configurations: square antiprism (SAPR-8, D_{4d}), dodecahedron (DD-8, D_{2d}), or bicapped trigonal prism (BTP-8, C_{2v}), rearrangements between which have been found to be almost barrierless [15]. Moreover, the polytopal configuration strongly influences the exact d-orbitals arrangement (Scheme 5) [15(d)].

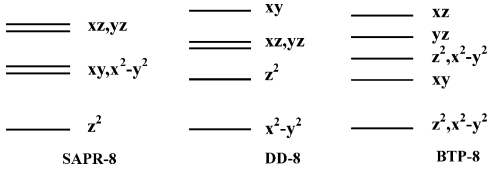

Scheme 5. Ref. [15(d)].

Generally, the octacyano-bridged systems can be divided into two main groups: (i) constructed with $[M^{V}(CN)_8]^{3-}$ building blocks, where M = Mo or W, which bear the spin $S = 1/2$ generating magnetic exchange through the cyano bridges, and (ii) built with diamagnetic ($S = 0$) $[M^{IV}(CN)_8]^{4-}$ anionic precursors, which in a few cases display photomagnetic properties.

The formation of M–CN–M′ links in the self-assembly reaction is accompanied by weaker interactions, like π–π stacking between aromatic rings, hydrogen bonds and/or electrostatic attraction. Therefore, the topology of the coordination network is determined not only by the geometries of building blocks but also by the nature of ligands and solvents.

2.3. IR cyanide characteristics

The presence of cyano ligands results in ν(CN) absorption in the infra-red spectra of the systems build by $[M(CN)_8]^{3-/4-}$ moieties. The C–N stretching mode frequencies are influenced by the sum of three main effects: (i) electron density withdrawal from sp σ* MO of the CN ligand by one (terminal cyano ligand) or two metal centres (bridging cyano ligand) causing an increase of ν(CN) frequency, (ii) the backdonation to p π* MO of CN ligand decreasing the stretching frequency, and (iii) kinematic coupling in the M–CN–M′ unit increasing the ν(CN) frequency [16]. Moreover, the exact position, number and intensity of ν(CN) bands is very sensitive to the oxidation state of the M and M′ metal centre, geometry of the bridging unit, countercations and solvents present in the crystal lattice. The experimental IR data indicate that the range characteristic for terminal cyano ligands in $[M(CN)_8]^{4-}$ ions of 2070–2130 cm^{-1} is shifted to 2130–2170 cm^{-1} for $[M(CN)_8]^{3-}$ [17]. The formation of M–CN–M′ bridges causes a further shift to the maximum values of 2166 and 2236 cm^{-1} for bridged assemblies based on $[M(CN)_8]^{4-}$ and $[M(CN)_8]^{3-}$ ions, respectively. Exceptions from these general rules are often observed in systems containing strongly electron withdrawing ligands, such as Schiff bases, where the bridging ν(CN) bands are in the range characteristic for the terminal ligands in $[M(CN)_8]^{3-/4-}$ ions. This phenomenon can be explained by stronger electron withdrawing from M′ metal centre by terminal ligands which causes enhanced backdonation to the CN bridge and compensates the kinematic coupling. The complete set of experimental ν(CN) frequencies for ionic and cyano-bridged $[M(CN)_8]^{3-/4-}$ assemblies has been presented elsewhere [7].

2.4. Magnetism: basic relationships

Octacyanometalates are excellent building blocks for constructing molecular magnetic materials because the cyanide ligand efficiently connects spin densities at metal centres through d π(M)–p π*(CN)–d π(M′) interactions in the M–CN–M′ bridge. The sign and magnitude of local exchange interactions can be tuned by systematic variation of 3d- or 4f-metal centres and blocking ligands.

The magnetic interaction between two paramagnetic centres can be considered in terms of the phenomenological Heisenberg

Hamiltonian (Eq. (1)):

$$\hat{H} = -J\sum_{M'} \hat{S}_M \hat{S}_{M'} + \beta g H \hat{S}_{Tz} - zJ'\langle \hat{S}_{Tz}\rangle \hat{S}_{Tz}, \quad (1)$$

where J is known as an intramolecular coupling constant, $\hat{S}_M$ and $\hat{S}_{M'}$ denote the spin operators of the paramagnetic centres and, assuming the magnetic field (H) to be along the z-direction, $\hat{S}_{Tz}$ is the z component of the total spin operator. Including the intermolecular coupling constant J' with the z nearest neighbours in the crystal lattice, the magnetic susceptibility of the polynuclear system $\chi_M T$ is expressed by the following formula (Eq. (2)):

$$\chi_M T = \chi_{mol} T/(1 - \chi_{mol} z J'/N g^2 \beta^2), \quad (2)$$

where χ_{mol} denotes the magnetic susceptibility of the polynuclear molecule being a function of the J coupling constant.

The total magnetic interaction is the sum of two contributions: positive ferromagnetic J_F and negative antiferromagnetic J_{AF} coupling [18]. Therefore, the J coupling constant indicating the nature of magnetic interaction can be expressed as $J = J_F + J_{AF}$. The two existing orbital models, Hoffmann's model (orthogonalized magnetic orbitals) and Kahn's model (non-orthogonalized magnetic orbitals), assume that the orthogonal orbitals cause ferromagnetism and the overlapping orbitals give rise to the antiferromagnetic contribution [19,20]. In the case of magnetic coupling between paramagnetic centres bearing several electrons, n_M and $n_{M'}$, the exchange pathways are described by the following expression (Eq. (3)) [21]:

$$J = \left(\sum_i \sum_j J_{ij}\right)/n_M n_{M'}. \quad (3)$$

When two interacting sites are ferromagnetically coupled the total ground state spin S_T is equal to $S_T = S_M + S_{M'}$; the antiferromagnetic coupling provides the total spin equal to $S_T = |S_M - S_{M'}|$.

2.5. Photomagnetism: general description

Photomagnetism, in general, includes such effects as photoinduced magnetization or photodemagnetization. It is constituted by the changes of magnetic properties resulting from the photoinduced electron transfer between two spin carriers, light induced excited spin state trapping or valence tautomerism [22]. The photoinduced valence tautomeric interconversion in the series of Prussian blue analogues has been widely explored [23]. The tautomeric equilibrium for one of the Prussian blue-like networks is shown in the following equation:

$$\underset{S=0}{Fe_{(LS)}^{II}}\text{–CN–}\underset{S=0}{Co_{(LS)}^{III}} \leftrightarrows \underset{S=1/2}{Fe_{(LS)}^{III}}\text{–CN–}\underset{S=3/2}{Co_{(HS)}^{II}} \quad (4)$$

where the cyano-bridged local pair on the left side is diamagnetic while the right side of the equation presents the paramagnetic pair with possible magnetic coupling [24,25].

The use of octacyanometalates in the construction of new photomagnetic materials is a natural extension of the strategy applied in the Prussian blue analogues. The outer-sphere metal-to-metal charge transfer (OS MMCT) photochemistry of

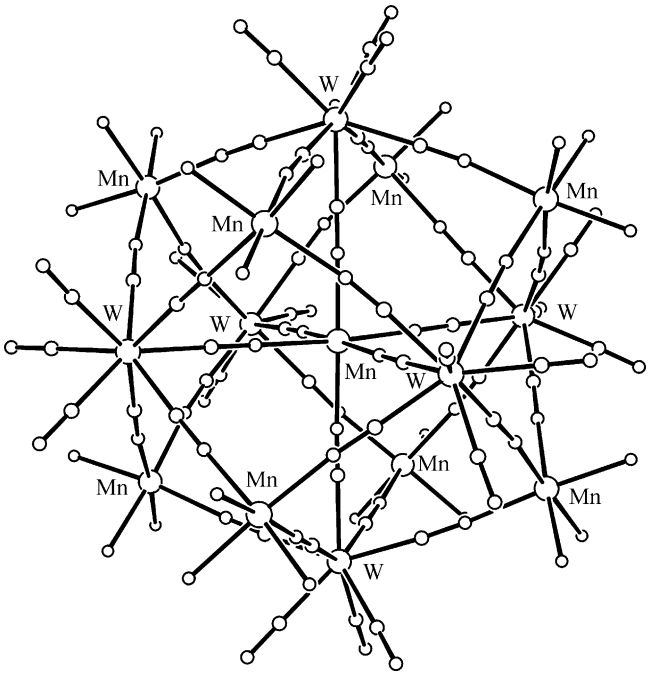

Fig. 1. Molecular structure of $[Mn^{II}\{Mn^{II}(EtOH)_3\}_8\{W^V(CN)_8\}_6]\cdot 12EtOH$ (hydrogen atoms and carbon atoms of ethanol molecules omitted for clarity). Reprinted with permission from Ref. [28]. Copyright 2000 American Chemical Society.

$[M(CN)_8]^{4-}$-based ion pairs (see Scheme 4) seems to be a starting point towards the rational design of light-switchable supramolecular materials. The photoinduced electron transfer in the systems containing diamagnetic $[M^{IV}(CN)_8]^{4-}$ building blocks gives the paramagnetic octacyanometalate(V) centre magnetically coupled with the cyano-bridged M′ metal centres: M^{IV}–CN–$M'^{n+} \rightarrow M^V$–CN–$M'^{(n-1)+}$. If the photomagnetic effect is reversible then the starting material is restored by the thermal pathway.

3. 0D bimetallic assemblies

The zero-dimensional cyano-bridged bimetallic assemblies are represented by discrete polynuclear molecules and ions. They are very promising materials of potential application in microelectronics, information storage or quantum computing as spin carriers. In this context, the polynuclear high-spin clusters and reversible photomagnets attract special attention.

The highest ground state spin value of the cyano-bridged system reported to date is displayed by two isostructural pentadecanuclear molecules: $[Mn^{II}\{Mn^{II}(MeOH)_3\}_8\{Mo^V(CN)_8\}_6]\cdot 5MeOH\cdot 2H_2O$ [26,27] and $[Mn^{II}\{Mn^{II}(EtOH)_3\}_8\{W^V(CN)_8\}_6]\cdot 12EtOH$ [27,28]. In the Mn_9M_6 (M = Mo, W) clusters, nine Mn(II) and six M(V) centres are arranged in a 'full-capped cubane' (Fig. 1). One of the Mn(II) centres is situated in the middle of the cluster with six nitrogen bonded cyano ligands in an almost ideal octahedral arrangement. Each of the $[M(CN)_8]^{3-}$ ions has five bridging cyano ligands, and the Mn(II) centres located in 'corners' of the molecule have three N-bonded CN ligands each. The antiferromagnetic coupling corresponding to

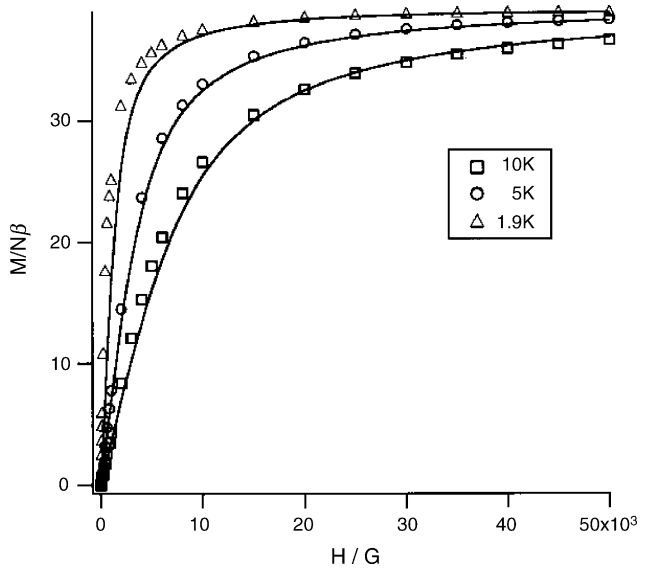

Fig. 2. Field dependence of magnetization for $[Mn^{II}\{Mn^{II}(EtOH)_3\}_8\{W^V(CN)_8\}_6]\cdot 12EtOH$ in different temperatures. Brillouin functions for $S = 39/2$ and $g = 2.0$ (solid lines). Reprinted with permission from Ref. [28]. Copyright 2000 American Chemical Society.

antiparallel arrangement of all Mn(II) spins with all M(V) spins gives rise to the total spin equal to $S = 39/2$. The Brillouin function fitted with $S = 39/2$ and $g = 2.00$ to the M versus H data measured at 1.9 K confirms the antiferromagnetic coupling for Mn_9W_6 cluster (Fig. 2).

Further studies on 0D octacyano-based systems resulted in the synthesis and characterization of several polynuclear molecules with magnetically coupled metal centres: the cobalt(II) analogues of Mn_9M_6 $[Co^{II}\{Co^{II}(MeOH)_3\}_8\{W^V(CN)_3\}_6]\cdot 19H_2O$ and $[Co^{II}\{Co^{II}(MeOH)_3\}_8\{Mo^V(CN)_3\}_6]\cdot 4MeOH\cdot 16H_2O$ (ground state $S = 21/2$) [29], a pentadecanuclear $[Ni^{II}\{Ni^{II}(MeOH)_3\}_8\{W^V(CN)_3\}_6]\cdot 15MeOH$ and $[Ni^{II}\{Ni^{II}(MeOH)_3\}_8\{Mo^V(CN)_3\}_6]\cdot 17MeOH\cdot H_2O$ (ground state $S = 12$) [30], octadecanuclear $[\{Ni^{II}L^1\}_{12}\{Nb^{IV}(CN)_8\}_6(H_2O)_6]\cdot 100H_2O$ [31], a pentanuclear $[Mn^{II}(2,2'\text{-bpy})_2][Mn^{II}(2,2'\text{-bpy})_2(H_2O)]_2[W^V(CN)_8]_2\cdot 7H_2O$ ($S = 13/2$) [32] and tetranuclear molecule with the spin reorientation $[Mn^{III}(salen)(H_2O)]_3[W^V(CN)_8]\cdot H_2O$ (ground state $S = 3/2$) [33], as well as dinuclear species: $[Cu^{II}(L^2)]_3[W^V(CN)_8]_2\cdot 4H_2O$ [34], $[Ni^{II}(en)_3]\{[Ni^{II}(en)_2(H_2O)][Mo^{IV}(CN)_8]\}\cdot 2H_2O$ [35] and $[Mn^{III}(3\text{-}OMesalophen)(H_2O)_2]_2\{[Mn^{III}(3\text{-}OMesalophen)(H_2O)]\}[W^V(CN)_8]\cdot 2H_2O$ [36].

The *spin-flop* phenomenon is represented by the magnetic behaviour of the tetranuclear molecule $[Mn^{III}(salen)(H_2O)]_3[W^V(CN)_8]\cdot H_2O$ [33]. In the V-shaped molecule, metal centres are linked through two cyano bridges and one single phenolate bridge (Fig. 3). Antiferromagnetic coupling through the cyano ($J_1 = -1.5\,cm^{-1}$) and phenolate ($J_2 = -3.9\,cm^{-1}$) bridges provides the ground state spin of $S = 3/2$. The energy spectrum of spin levels in an external magnetic field for the Mn_3W molecule shows the intersection between $S = 3/2$ and 5/2 states at $H \sim 28$ kOe which gives rise to the *spin-flop* transition (Fig. 4).

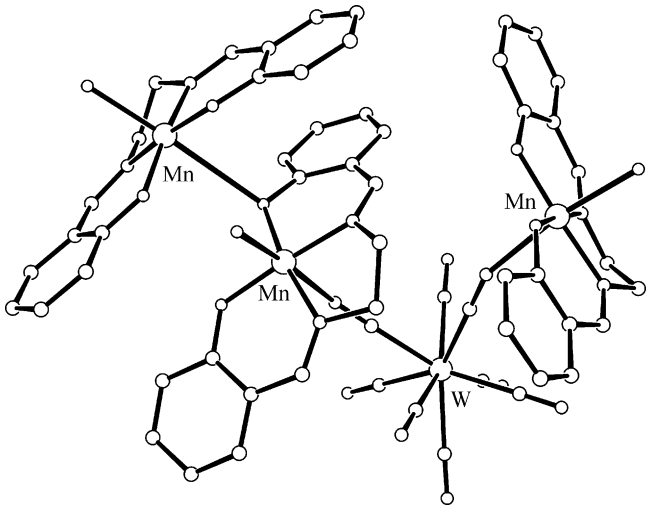

Fig. 3. Asymmetric unit of $[Mn^{III}(salen)(H_2O)]_3[W^V(CN)_8]\cdot H_2O$ (hydrogen atoms and water of crystallization omitted for clarity). Reprinted with permission from Ref. [33]. Copyright 2004 American Chemical Society.

A separate group of 0D assemblies based on diamagnetic $[M(CN)_8]^{4-}$ moieties is constituted by the photomagnetic materials in which the photoinduced electron transfer between metallic centres causes magnetic coupling in the photoproduct. In this group of compounds, structural and photomagnetic properties were reported for $[Mn^{II}(2,2'\text{-bpy})_2]_4[M^{IV}(CN)_8]_2\cdot 8H_2O$ (M = Mo, W) [37,38], $[Cu^{II}(2,2'\text{-bpy})_2]_2[Mo^{IV}(CN)_8]\cdot 5H_2O\cdot MeOH$ [39] and $[Cu^{II}(tren)]_6[Mo^{IV}(CN)_8](ClO_4)_8\cdot 4.5H_2O$ [40].

The heptanuclear cluster $[Cu^{II}(tren)]_6[Mo^{IV}(CN)_8](ClO_4)_8\cdot 4.5H_2O$ displays reversible photomagnetism after irradiation

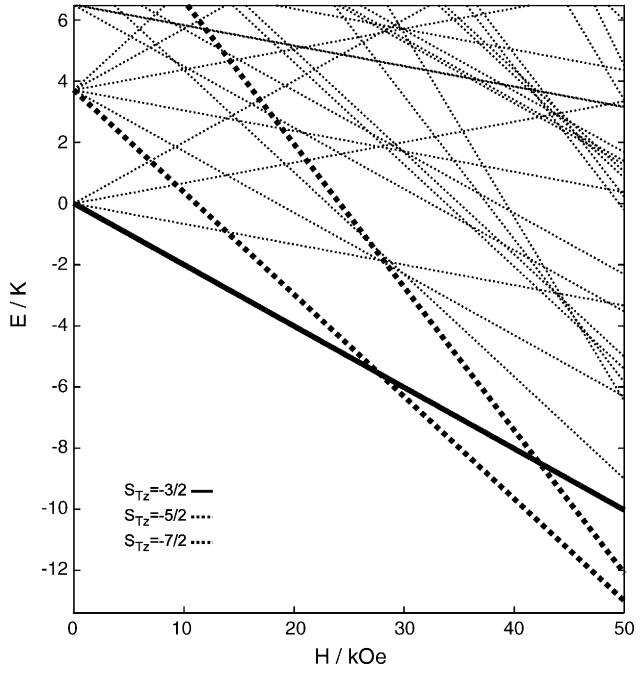

Fig. 4. Energy spectrum of an isolated unit of $[Mn^{III}(salen)(H_2O)]_3[W^V(CN)_8]\cdot H_2O$ in an external magnetic field. Reprinted with permission from Ref. [33]. Copyright 2004 American Chemical Society.

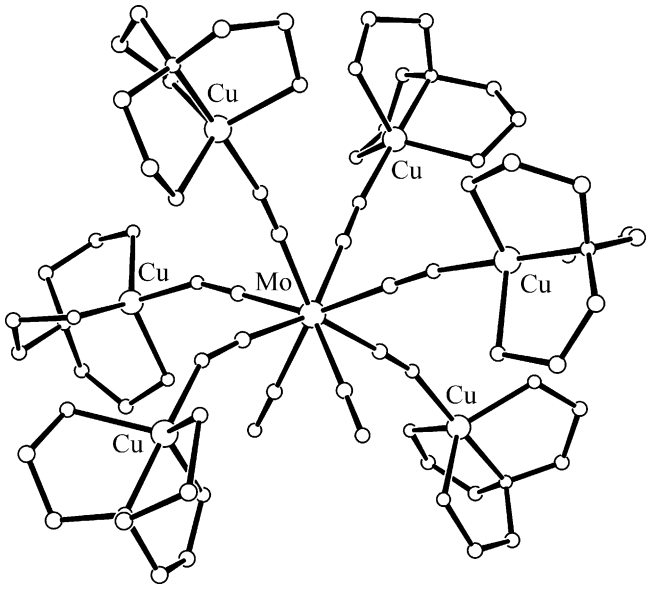

Fig. 5. X-ray structure of $[Cu^{II}(tren)]_6[Mo^{IV}(CN)_8](ClO_4)_8{\cdot}4.5H_2O$ (hydrogen atoms, water of crystallization and counterions omitted for clarity). Reprinted with permission from Ref. [40]. Copyright 2004 Wiley/VCH.

[40]. The $\{[Cu(tren)]_6[Mo(CN)_8]\}^{8+}$ ion consists of six Cu(II) centres linked to the Mo(IV) centre through single cyano bridges (Fig. 5). The $\{[Cu(tren)]_6[Mo(CN)_8]\}^{8+}$ ion is characterized by the MMCT transition at 440 nm. The magnetic measurements performed before and after irradiation with blue light (406–415 nm) show a reversible photomagnetic effect in the heating mode (Fig. 6). Irradiation near to the MMCT band produces a $Mo^{V}Cu^{I}Cu_5^{II}$ photoproduct containing a Mo(V) paramagnetic centre which gives rise to the ferromagnetic coupling through the CN bridges with five Cu(II) centres resulting in the total spin $S = 3$.

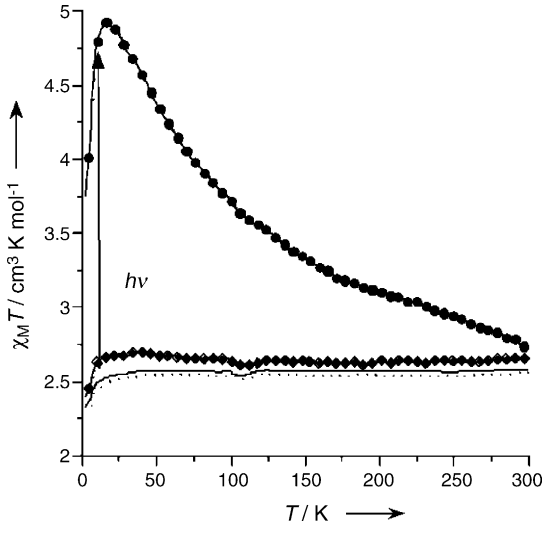

Fig. 6. Thermal dependence of the $\chi_M T$ for $[Cu^{II}(tren)]_6[Mo^{IV}(CN)_8](ClO_4)_8{\cdot}4.5H_2O$: (·) before irradiation, (●) after irradiation, and (♦) after irradiation and $T > 300$ K. Reprinted with permission from Ref. [40]. Copyright 2004 Wiley/VCH.

The structural and magnetic characterization summary for 0D octacyano-based systems is presented in Table 1. The octacyanometalate-based systems are characterized by practically linear M–CN bonds. The structural archetype of M'_9M_6 clusters based on solvated M′ sites exhibits a close to linear M′–NC motif (mean value of 176.5°). The presence of blocking ligands at M′ centre in other systems cause significant bending of M′–NC bridges (mean value of 160.0°) due to the introduced steric hindrance. Regardless of the metric parameters of Mn–NC–M and the oxidation state of Mn centre, the Mn(II, III)-based 0D systems invariably exhibit intramolecular antiferromagnetic interactions.

The chelated Cu(II) sites are five-coordinate and form only one Cu–NC–M bridge in 0D compounds. Its metric parameters determine the nature and magnitude of the magnetic interactions. Axial coordination of long and bent cyano bridges to Cu(II) square pyramidal site results in ferromagnetic coupling in $[Cu^{II}(L^2)]_3[W^{V}(CN)_8]_2{\cdot}4H_2O$ [34]. In photomagnetic $[Cu^{II}(2,2'\text{-bpy})_2]_2[Mo^{IV}(CN)_8]{\cdot}5H_2O{\cdot}MeOH$ molecule shorter equatorial cyano bridges in trigonal bipyramidal Cu(II) site cause an antiferromagnetic interaction between photogenerated Mo(V) and Cu(II) [39]. However, axial coordination of CN bridge to Cu(II) of trigonal bipyramidal geometry in $[Cu^{II}(tren)]_6[Mo^{IV}(CN)_8](ClO_4)_8{\cdot}4.5H_2O$ results in ferromagnetic coupling between photoinduced Mo(V) and Cu(II) [40].

4. 1D bimetallic assemblies

The octacyanometalate moiety coupled with 3d and 4f metal complexes propagates efficiently in one direction to form chains of different topologies. $[Mn_2^{II}(L^3)_2(H_2O)][Mo^{IV}(CN)_8]{\cdot}5H_2O$ forms a 1D zigzag bimetallic chain [42]. There are two topologically different Mn coordination sites in the structure. One forms two *trans*-cyano bridges developing the polymeric structure, while another coordinates one cyano bridge, acting as a pendant arm. The alternating bimetallic chain behaves as a paramagnet at room temperature, due to the long Mn^{II}–Mn^{II} distance, which is larger than 9 Å. Magnetization versus field reaches a saturation value of 9.75 Nβ at 50 kOe and $\chi_M T$ value of 8.74 emu K mol^{-1}, which remains nearly constant within the range of 2–300 K. This compound exhibits irreversible photomagnetic effect under the irradiation with UV light for 10 h. The photooxidation of Mo^{IV}–Mo^{V} causes a small, but noticeable increase in $\chi_M T$ value at room temperature up to 9.14 emu K mol^{-1}. On lowering the temperature the $\chi_M T$ curve shifts up, reaching a maximum of 21.2 emu K mol^{-1} at 4 K and then falls down, which indicates the presence of antiferromagnetic coupling between Mn^{II} and Mo^{V} centres at low temperature. The field dependence of magnetization reaches the saturation value of 8.96 Nβ at 2 K, which corresponds to the antiferromagnetic coupling between two $S = 5/2$ spins and one $S = 1/2$ spin.

The self-assembly of $[Mn^{III}(salen)(H_2O)]^+$ and $[Mo^{IV}(CN)_8]^{4-}$ in aqueous solution leads to the formation of the 1D $[Mn^{III}(salen)(H_2O)_2]_2\{[Mn^{III}(salen)(H_2O)][Mn^{III}(salen)]_2[Mo^{IV}(CN)_8]\}{\cdot}0.5ClO_4{\cdot}0.5OH{\cdot}4.5H_2O$ chain built by the single cyano-bridged $\{[Mn^{III}(salen)(H_2O)][Mn^{III}(salen)]_2[Mo^{IV}(CN)_8]\}$ units which propagate into the 1D array by dou-

Table 1
Relevant geometric parameters and magnetic properties for 0D bimetallic assemblies

Compound	$[M(CN)_8]^{3-/4-}$ geometry	Number of M–CN bridges	C–M–C angle (°)[a]	M′ site geometry	Number of M′–NC bridges	M′–N bond length (Å)	M′–N–C angle (°)	Magnetic properties	Reference
$[Mn^{II}\{Mn^{II}(MeOH)_3\}_8\{Mo^{V}(CN)_8\}_6]\cdot 5MeOH\cdot 2H_2O$	DD-8[b]	5	145.50	OC-6	6	2.184(5)	178.1(5)	AF giving a total spin $S = 39/2$	[26,27]
			142.6(2)			2.190(5)	179.2(5)		
						2.182(5)	175.9(4)		
	DD-8[b]	5	144.7(2)	OC-6	3	2.195(6)	173.9(6)		
			144.1(2)			2.190(6)	177.6(5)		
						2.209(6)	174.6(6)		
	DD-8[b]	5	143.0(2)	OC-6	3	2.201(6)	173.7(5)		
			144.4(2)			2.222(6)	172.0(5)		
						2.208(6)	173.0(5)		
				OC-6	3	2.218(6)	174.0(5)		
						2.225(5)	174.1(5)		
						2.207(6)	170.9(5)		
				OC-6	3	2.214(6)	169.6(5)		
						2.193(6)	178.8(5)		
						2.207(6)	175.4(6)		
$[Mn^{II}\{Mn^{II}(EtOH)_3\}_8\{W^{V}(CN)_8\}_6]\cdot 12EtOH$	BTP-8	5	146.2(5)	OC-6	6	2.22(1)	167(1)	AF giving a total spin $S = 39/2$	[27,28]
			71.6(5)	OC-6	3	2.20(1)	173(1)		
				OC-6	3	2.19(1)	170(1)		
						2.21(1)	162(1)		
$[Mn^{II}(2,2'\text{-bpy})_2]_4[Mo^{IV}(CN)_8]_2\cdot 14H_2O$	SAPR-8	4	116.2(2)	OC-6	2	2.179(5)	172.8(6)	Photomagnetic; AF photoproduct after irradiation	[37,38]
			111.7(3)			2.142(6)	153.3(6)		
				OC-6	2	2.156(6)	162.5(6)		
						2.130(6)	155.7(6)		
$[Mn^{II}(2,2'\text{-bpy})_2][Mn^{II}(2,2'\text{-bpy})_2(H_2O)]_2[W^{V}(CN)_8]_2\cdot 7H_2O$	SAPR-8	2	135.8(2)	OC-6	2	2.222(6)	162.7(6)	AF coupling between W^{v} and Mn^{II} with a total spin $S = 13/2$	[32]
						2.192(6)			
				OC-6	1	2.192(6)	163.7(6)		
$[Mn^{III}(salen)(H_2O)]_3[W^{V}(CN)_8]\cdot H_2O$	SAPR-8	2	72.74(12)	OC-6	1	2.336(3)	153.2(3)	AF with $J_1 = -1.5\,cm^{-1}$, $J_2 = -3.9\,cm^{-1}$ and $J' = -0.7\,cm^{-1}$	[33]
				OC-6	1	2.398(3)	149.3(3)		
$[Mn^{III}(3\text{-OMesalophen})(H_2O)_2]_2\{[Mn^{III}(3\text{-OMesalophen})(H_2O)]\}[W^{V}(CN)_8]\cdot 2H_2O$	SAPR-8	1		OC-6	1	2.325(8)	159.4(7)	AF with $J_1 = -20\,cm^{-1}$, $J_2 = -0.46\,cm^{-1}$ and $D = -4.0\,cm^{-1}$	[36]
$[Ni^{II}\{Ni^{II}(MeOH)_3\}_8\{Mo^{V}(CN)_3\}_6]\cdot 17MeOH\cdot H_2O$	BTP-8	5	145.36(16)	OC-6	6	2.034(3)	176.4(3)	F with a total spin $S = 12$	[30]

			142.62(15)			2.039(3)	179.2(4)		
	BTP-8	5	142.56(16)			2.046(3)	175.7(3)		
			146.11(16)	OC-6	3	2.052(4)	174.9(4)		
	DD-8	5	144.21(16)			2.042(4)	177.7(4)		
			143.53(15)			2.049(4)	175.3(3)		
				OC-6	3	2.050(4)	177.4(4)		
						2.054(4)	174.1(4)		
						2.042(4)	176.4(4)		
				OC-6	3	2.066(4)	178.4(4)		
						2.057(4)	174.3(3)		
						2.054(4)	174.3(3)		
				OC-6	3	2.038(4)	174.7(3)		
						2.051(4)	175.9(4)		
						2.057(4)	171.8(3)		
$[Ni^{II}\{Ni^{II}(MeOH)_3\}_8\{W^V(CN)_3\}_6]\cdot 15MeOH$	BTP-8	5	Isostructural to Ni_9Mo_6	OC-6	6	Isostructural to Ni_9Mo_6	Isostructural to Ni_9Mo_6	F with a total spin $S = 12$	[30]
	BTP-8	5		OC-6	3				
	DD-8	5		OC-6	3				
				OC-6	3				
				OC-6	3				
$[Ni^{II}(en)_3]\{[Ni^{II}(en)_2(H_2O)][Mo^{IV}(CN)_8]\}\cdot 2H_2O$	SAPR-8[b]	1		OC-6	1	2.075(4)	158.7(3)	Very weak AF	[35]
$[\{Ni^{II}L^1\}_{12}\{Nb^{IV}(CN)_8\}_6(H_2O)_6]\cdot 100H_2O$	DD-8	3	122.4(9)	OC-6	2	2.12(2)	169(3)	AF	[31]
			79.2(9)			2.10(2)	145(2)		
			144.0(9)	OC-6	1	2.06(2)	165(2)		
$[Co^{II}\{Co^{II}(MeOH)_3\}_8\{W^V(CN)_8\}]\cdot 19MeOH$	DD-8[b]	5	144.5(2)	OC-6	6	2.60(5)	173.9(5)	AF with total spin $S = 21/2$	[29]
			141.7(2)			2.079(5)	179.2(5)		
	DD-8[b]	5	143.1(2)			2.091(5)	177.2(5)		
			144.9(2)	OC-6	3	2.077(5)	175.1(5)		
	DD-8[b]	5	145.1(2)			2.082(6)	176.1(5)		
			142.7(7)			2.098(5)	173.6(5)		
				OC-6	3	2.099(5)	175.3(5)		
						2.120(6)	173.7(5)		
						2.117(6)	171.7(5)		
				OC-6	3	2.057(5)	173.5(5)		
						2.075(6)	179.2(6)		
						2.087(6)	175.5(5)		
				OC-6	3	2.071(6)	177.2(5)		
						2.086(5)	176.4(5)		
						2.082(6)	176.8(6)		

Table 1 (*Continued*)

Compound	$[M(CN)_8]^{3-/4-}$ geometry	Number of M–CN bridges	C–M–C angle (°)[a]	M′ site geometry	Number of M′–NC bridges	M′–N bond length (Å)	M′–N–C angle (°)	Magnetic properties	Reference
$[Co^{II}\{Co^{II}(MeOH)_3\}_8\{Mo^{V}(CN)_8\}]\cdot 4MeOH\cdot 16H_2O$	DD-8[b]	5	143.09(16)	OC-6	6	2.074(4)	175.4(3)	AF with total spin $S = 21/2$	[29]
			144.76(16)			2.079(4)	177.2(4)		
	DD-8[b]	5	145.09(16)			2.082(4)	178.5(3)		
			144.67(16)	OC-6	3	2.072(4)	176.2(3)		
	DD-8[b]	5	143.26(16)			2.091(4)	175.9(4)		
			144.15(17)			2.123(4)	173.3(4)		
				OC-6	3	2.081(4)	176.0(4)		
						2.094(4)	173.8(3)		
						2.120(4)	176.7(4)		
				OC-6	3	2.066(4)	179.5(5)		
						2.084(4)	173.3(3)		
						2.086(4)	177.4(4)		
				OC-6	3	2.079(4)	178.0(4)		
						2.101(4)	176.6(4)		
						2.109(4)	175.4(3)		
$[Cu^{II}(tren)]_6[Mo^{IV}(CN)_8](ClO_4)_8\cdot 4.5H_2O$	DD-8	6	106.4(2)	TBPY	1	1.891(5)ax	149.3(5)	Reversible photomagnet; F after irradiation	[40]
			105.68(19)			1.987(5)ax	172.5(5)		
			75.56(18)						
			102.0(3)						
			112.4(2)						
			77.6(2)						
$[Cu^{II}(2,2'\text{-bpy})_2]_2[Mo^{IV}(CN)_8]\cdot 5H_2O\cdot MeOH$	DD-8	2	144.6(2)	TBPY-5	1	1.963(4)eq	161.3(4)	Photomagnetic; after irradiation	[39]
				TBPY-5	1	1.973(4)eq	166.6(5)	AF coupled three spins $S = 1/2$	
$[Cu^{II}(L^2)]_3[W^{V}(CN)_8]_2\cdot 4H_2O$	SAPR-8[b]		74.1(2)	SPY-5	1	2.300(5)ax	161.1(5)	F	[34]
				SPY-5	1	2.209(5)ax	169.3(8)		
	SAPR-8[b]			SPY-5	1	2.368(4)ax	147.5(4)		

[a] The C–M–C angles in the $[M(CN)_8]^{3-/4-}$ moiety.
[b] Geometry determined using the program SHAPE [41].

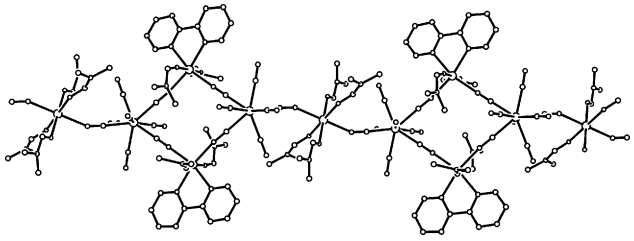

Fig. 7. Molecular structure of $[Mn_3^{II}(2,2'\text{-bpy})_2(DMF)_8][W^V(CN)_8]_2$ (hydrogen atoms omitted for clarity). Reprinted with permission from Ref. [44]. Copyright 2003 American Chemical Society.

ble phenolate bridges [33]. Magnetic measurements reveal nearly paramagnetic behaviour with very weak antiferromagnetic interaction between Mn(III) centres through the phenolate-bridges.

$\{[Mn^{II}(2,2'\text{-bpy})(DMF)_2]_2[Mo^V(CN)_8]_2[Mn^{II}(DMF)_4]\}_\infty$ is an example of 1D structure of 3,2-chain topology [43,44]. The structure consists of two types of Mn centres, forming two cyano bridges (Fig. 7). Each $[Mn^{II}(2,2'\text{-bpy})(DMF)_2(NC)_2]$ possesses cyano ligands in *cis* position and forms a quadrinuclear unit, whereas *trans*-$[Mn^{II}(DMF)_4(NC)_2]$ acts as a spacer between these squares. The structure of the assembly contains paramagnetic Mn(II) and Mo(V) centres connected by short and linear as well as longer and more bent cyano bridges. Magnetic measurements reveal antiferromagnetic coupling between metal centres as well as long-range magnetic ordering in low temperature. The $\chi_M T$ value at room temperature of 13.84 emu K mol^{-1} reproduces the spin only value expected for $Mn_3^{II}Mo_2^V$ unit. With the decrease of temperature, $\chi_M T$ curve reaches a minimum near 60 K, which suggests the presence of weak antiferromagnetic interactions, and then increases up to maximum at 4.8 K. Field-cooled magnetization measurements exhibit a dramatic increase near 3.2 K, which suggest spontaneous magnetization. AC magnetic susceptibility measurements performed at different field frequencies show the presence of χ'_M maximum near 2.8 K, which confirms the long-range ferrimagnetic ordering below that temperature (Fig. 8). The assembly behaves like a soft magnet with coercive field of 10 Oe.

The octacyanotungstate(V)-based cyano-bridged 1D polymer $\{[Mn_3^{II}(2,2'\text{-bpy})_2(DMF)_8][W^V(CN)_8]_2\}_\infty$ is isostructural with its molybdate analogue [44]. The magnetic properties of the assembly are similar; it displays the presence of long-range ferrimagnetic interactions below 3.5 K and glassy behaviour.

One of the few coordination polymers based on cobalt and octacyanometallates, $\{[Co_3^{II}(DMF)_{12}][W^V(CN)_8]_2\}_\infty$, reveals 1D structure of similar 3,2-chain topology [44]. Each cobalt site of distorted octahedral geometry coordinates four dimethylformamide ligands and two cyano ligands (Fig. 9). Depending on mutual orientation of cyano bridges, there are *cis*-bridging units, forming the tetrametallic squares Co_2W_2 and *trans*-bridging units, linking squares into 1D array. Magnetic susceptibility versus temperature fits the Curie–Weiss law with $g_W = 2.0$, $g_{Co} = 2.84$ and $\theta = 14.44$ K and indicates the presence of ferromagnetic coupling. The $\chi_M T$ curve jumps from a room temperature value of 12.68 to 46.78 emu K mol^{-1} at 14 K. The presence

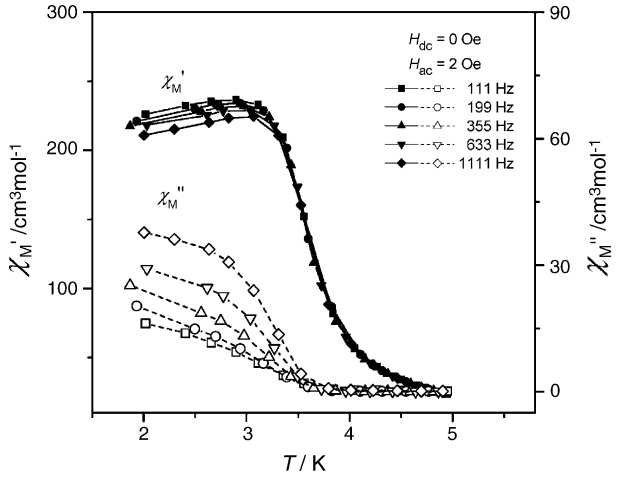

Fig. 8. Temperature dependence of zero-field ac susceptibility for $[Mn_3^{II}(2,2'\text{-bpy})_2(DMF)_8][W^V(CN)_8]_2$. Reprinted with permission from Ref. [44]. Copyright 2003 American Chemical Society.

of long-range magnetic ordering can also be seen through the FCM and ZFCM measurements, which show different behaviour below 10 K. AC susceptibility studies show that the maximum of χ'_M is located between 6 and 8 K, depending on field frequency. The temperature of the transition is estimated as 7.3 K from the positions of maxima of second harmonics. Magnetization versus field measurements clearly show saturation near 11 Nβ expected for ferromagnetically coupled three $S = 3/2$ and two $S = 1/2$ spins. The hysteresis loop is characterized by rather large coercive field 907 Oe and remnant magnetization of 3.39 Nβ (Fig. 10).

The 1D $[\{Mn^{II}L^3\}_2\{Nb^{IV}(CN)_8\}(H_2O)]_\infty$ is based on a Mn(II) complex with the macrocycle ligand coordinated by five nitrogen atoms [31]. The structure and topology of the assembly is analogous to that of $[Mn_2^{II}(L^3)_2(H_2O)][Mo^{IV}(CN)_8]\cdot 5H_2O$ [42]. The $\chi_M T$ value of the compound measured at room temperature is 8.85 emu K mol^{-1}, which is consistent with the value 9.125 emu K mol^{-1} anticipated for two Mn^{II} and one Nb^{IV} centres. In lower temperatures the curve decreases until 130 K and then shifts up dramatically which implies the presence of long-range magnetic correlation. Magnetization versus field curve measured at 2 K displays saturation value of 9 Nβ at 30 kOe, suggesting the presence of long-range antiferromagnetic coupling in the system.

The self-assembly of $[Mo^V(CN)_8]^{3-}$ and $[Cu^{II}(cyclam)]^{2+}$ resulted in the formation of the 1D coordination polymer

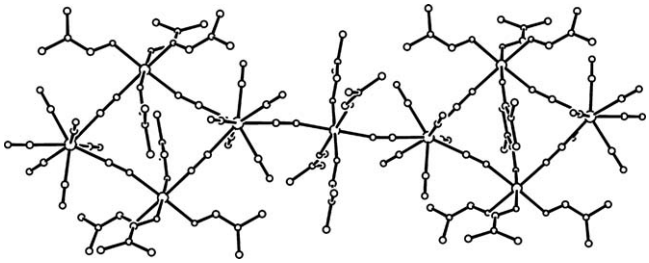

Fig. 9. Molecular structure of $[Co_3^{II}(DMF)_{12}][W^V(CN)_8]_2$ (hydrogen atoms omitted for clarity). Reprinted with permission from Ref. [44]. Copyright 2003 American Chemical Society.

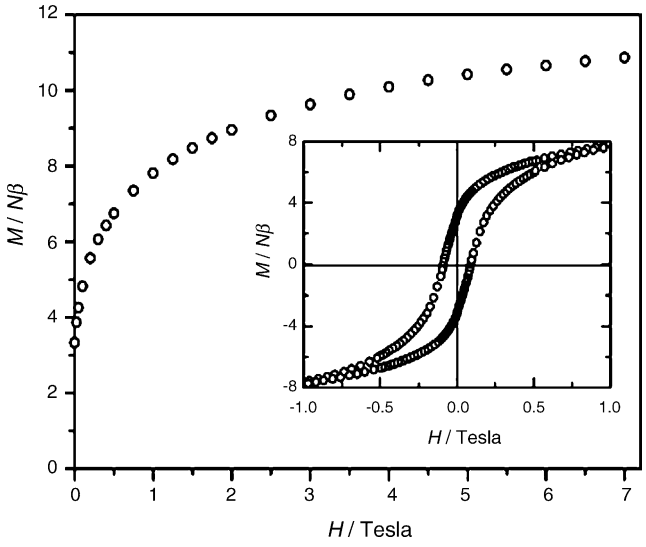

Fig. 10. Field dependence of the magnetization at 1.8 K for $[Co_3^{II}(DMF)_{12}][W^V(CN)_8]_2$ (inset: hysteresis loop at 1.8 K). Reprinted with permission from Ref. [44]. Copyright 2003 American Chemical Society.

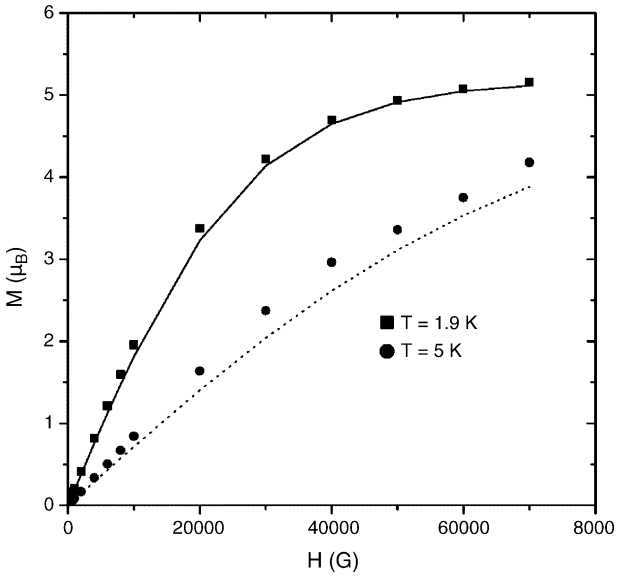

Fig. 12. Field dependence of the magnetization for $[Cu^{II}(cyclam)]_3[Mo^V(CN)_8]_2{\cdot}5H_2O$ with Brillouin functions (solid lines). Reprinted with permission from Ref. [45]. Copyright 2004 American Chemical Society.

$[Cu^{II}(cyclam)]_3[Mo^V(CN)_8]_2{\cdot}5H_2O$ [45]. The structure displays a rope ladder topology of the chain (Fig. 11). Octacyanomolybdate(V) ions act as nodes, forming three bridges towards copper(II) centres. Each $[Cu^{II}(cyclam)]^{2+}$ unit coordinates two cyano ligands in *trans* position, developing the structure of the ladder. The compound has a $\chi_M T$ value of 1.99 emu K mol^{-1} at room temperature, which corresponds to five $S = 1/2$ spins per one Cu_3Mo_2 unit. Upon cooling the curve shifts up and reaches the maximum value of 2.32 emu K mol^{-1}, which indicates ferromagnetic interaction. The Curie–Weiss law fit of χ_M^{-1} data gives $C = 1.99$ emu K mol^{-1} and $\theta = 1.24$ K. Magnetization versus field measured below 2 K shows a saturation value of 5 Nβ (Fig. 12). On the basis of the structural and magnetic data, the system can be treated as a set of ferromagnetic pentamers Cu_3Mo_2 coupled ferromagnetically within the chain. The presence of a weak interchain antiferromagnetic interaction has also been observed.

$[Cu^{II}(tetrenH_2)]_2[W^{IV}(CN)_8]_2{\cdot}5H_2O$ obtained from $[Cu^{II}(tetren)]^{2+}$ and $[W^V(CN)_8]^{3-}$ precursors exhibits a 1D chain structure. The compound behaves like a paramagnet, obeying the Curie–Weiss law with $C = 0.90$ emu K mol^{-1}, which confirms the presence of two spins $S = 1/2$ [46]. The interaction between paramagnetic copper(II) centres is described by $\theta = -0.33$ K,

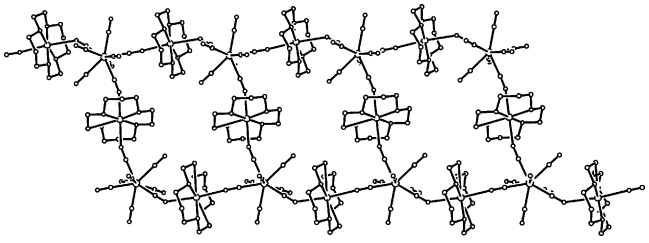

Fig. 11. One-dimensional chains of $[Cu^{II}(cyclam)]_3[Mo^V(CN)_8]_2{\cdot}5H_2O$ (hydrogen atoms and water of crystallization omitted for clarity). Reprinted with permission from Ref. [45]. Copyright 2004 American Chemical Society.

indicating rather poor contact of spins through diamagnetic $[W^{IV}(CN)_8]^{4-}$ spacers. Magnetization studies show clearly the presence of two uncoupled $S = 1/2$ spins per Cu_2W_2 unit.

Another 1D coordination network $[Cu^{II}(tetrenH)][Cu^{II}(tetrenH_2)]$ $[W^V(CN)_8][W^{IV}(CN)_8]_2{\cdot}2.5H_2O$ possesses partially reduced tungsten(V) centres [46]. The assembly was obtained from the same precursors as the previous one. Tuning of the self-assembly process by the pH value allowed the formation of a 1D chain structure of three-row ribbon pattern. The magnetic susceptibility of the compound fits the Curie–Weiss law with $C = 1.3$ emu K mol^{-1} and $\theta = -0.78$ K. The value of the Curie constant suggests the presence of spin $S = 1$ and $S = 1/2$ ($C = 1.375$ emu K mol^{-1}). Weak ferromagnetic coupling between Cu^{II} and W^V centres due to the formation of Cu^{II}–W^V–Cu^{II} bridges and stronger antiferromagnetic coupling, dominating at low temperature have been observed.

The new concept for construction of 1D chains with high-spin metal centres is based on the use of lanthanide(III) complexes as cationic building blocks in the self-assembly reaction with octacyanometalates. Recently reported $[Gd^{III}(DMF)_6][W^V(CN)_8]$ lanthanide-based system is an alternating 1D chain, which displays antiferromagnetic coupling between Gd(III) and W(V) metal centres [47(a)]. The use of 2,2′:6′,2″-terpyridine (terpy) results in the formation of $[Ln^{III}(terpy)(DMF)_4][W^V(CN)_8]{\cdot}6H_2O$ (Ln = Gd, Sm) with retention of the alternating 1D topology [47(b)]. Similarly to $[Gd^{III}(DMF)_6][W^V(CN)_8]$, the Gd(III) and W(V) centres are antiferromagnetically coupled. However, the $[Sm^{III}(terpy)(DMF)_4][W^V(CN)_8]{\cdot}6H_2O$ system exhibits the ferromagnetic intrachain interaction.

The relevant geometric parameters and magnetic properties summary for 1D octacyano-based systems are presented in Table 2. A 1D structure is obtained when the cationic building blocks bind to the cyano ligands which form C–M–C angles of

Table 2
Relevant geometric parameters and magnetic properties for 1D bimetallic assemblies

Compound	$[M(CN)_8]^{3-/4-}$ geometry	Number of M–CN bridges	C–M–C angle (°)[a]	M′ site geometry	Number of M′–NC bridges	M′–N bond length (Å)	M′–N–C angle (°)	Magnetic properties	Reference
$[Mn_2^{II}(L^3)_2(H_2O)][Mo^{IV}(CN)_8]\cdot 2H_2O$	SAPR-8	3	143.33(16)	PBPY-7	2	2.257(4)	151.3(3)	Photomagnetic (F ordering after irradiation)	[42]
						2.270(4)	143.3(3)		
				PBPY-7	1	2.243(4)	154.8(4)		
$\{[Mn^{II}(2,2'\text{-bpy})(DMF)_2]_2[Mo^{V}(CN)_8]_2[Mn^{II}(DMF)_4]\}_\infty$	BTP-8	3	72.89(13)	OC-6	2	2.181(3)	173.5(3)	AF	[43,44]
						2.191(3)	175.1(3)		
			136.11(13)	OC-6	2	2.251(3)	155.7(3)		
			125.00(13)						
$\{[Mn_3^{II}(2,2'\text{-bpy})_2(DMF)_8][W^{V}(CN)_8]_2\}_\infty$	BTP-8	3	124.4(4)	OC-6	2	2.215(1)	171.6(10)	Ferrimagnet with glassy behaviour	[44]
						2.180(1)			
				OC-6	2	2.254(9)	175.4(10)		
						2.254(9)	156.0(9)		
$[\{Mn^{II}L^3\}_2\{Nb^{IV}(CN)_8\}(H_2O)]_\infty$	SAPR-8	3	144.2(2)	OC-6	1	2.251(5)	154.7(5)	AF	[31]
			72.4(2)	OC-6	2	2.23(5)	150.5(5)		
			142.1(2)			2.268(6)	140.7(5)		
$[Mn^{III}(salen)(H_2O)_2]_2\{[Mn^{III}(salen)(H_2O)][Mn^{III}(salen)]_2$ $[Mo^{IV}(CN)_8]\}\cdot 0.5ClO_4\cdot 0.5OH\cdot 4.5H_2O$	SAPR-8	3	74.3(2)	OC-6	1	2.227(6)	150.2(5)	Nearly paramagnetic	[33]
			73.3(2)	OC-6	1	2.314(6)	152.0(6)		
			102.1(2)	OC-6	1	2.197(6)	142.7(5)		
$\{[Co_3^{II}(DMF)_{12}][W^{V}(CN)_8]_2\}_\infty$	BTP-8	3	130.41(15)	OC-6	2	2.131(3)	159.9(3)	F with long-range ordering and glassy behaviour	[44]
			137.54(15)			2.109(3)	158.2(3)		
			72.08(14)	OC-6	2	2.096(3)	167.7(4)		
$[Cu^{II}(cyclam)]_3[Mo^{V}(CN)_8]_2\cdot 5H_2O$	SAPR-8	3	76.07(14)	OC-6	2	2.711(4)	142.7(3)	F coupling with $J = 3.88\,cm^{-1}$ and $J' = -0.46\,cm^{-1}$	[45]
			139.52(14)			2.514(3)	160.6(3)		
			123.51(14)	OC-6	2	2.557(4)	156.6(3)		
$[Cu^{II}(tetrenH_2)]_2[W^{IV}(CN)_8]_2\cdot 5H_2O$	DD-8	3	74.3(4)	SPY-5	2	2.174(9)ax	154.3(8)	Paramagnetic	[46]
			71.9(3)			1.975(8)eq	171.1(8)		
	DD-8	2	124.7(4)	SPY-5	3	2.261(8)ax	146.5(8)		
			76.0(4)			1.961(9)eq	175.8(9)		
						2.82ax	148.6		
$[Cu^{II}(tetrenH_2)][Cu^{II}(tetrenH)][W^{V}(CN)_8][W^{IV}(CN)_8]\cdot 2.5H_2O$	SAPR-8	4	143.6(7)	OC-6	3	1.971(17)	167.1(14)	Very weak AF	[46]
			76.8(7)			2.431(18)	149.6(16)		
			112.8(8)			2.446(16)	175.2(19)		
			72.7(7)	OC-6	3	1.944(19)	172.1(17)		
			81.5(8)			2.287(16)	149.9(18)		

Table 2 (*Continued*)

Compound	$[M(CN)_8]^{3-/4-}$ geometry	Number of M–CN bridges	C–M–C angle (°)[a]	M′ site geometry	Number of M′–NC bridges	M′–N bond length (Å)	M′–N–C angle (°)	Magnetic properties	Reference
	SAPR-8	2	142.3(7) 116.6(8)			3.114(9)	148.4		
$[Gd^{III}(DMF)_6][W^{V}(CN)_8]$	SAPR-8	2	143.71	SAPR-8	2	2.540(8) 2.505(8)	172.4(8) 172.8(8)	AF with $J_1 = -0.58\,cm^{-1}$	[47(a)]
$[Gd^{III}(terpy)(DMF)_4][W^{V}(CN)_8]\cdot 6H_2O$	SAPR-8	2	144.37(15)	TTP-9	2	2.590(4) 2.559(4)	171.2(4) 170.3(4)	AF with $J = -2.3$ K	[47(b)]
$[Sm^{III}(terpy)(DMF)_4][W^{V}(CN)_8]\cdot 6H_2O$	SAPR-8	2	144.21(16)	TTP-9	2	2.603(4) 2.573(4)	177.6(4) 169.6(4)	F with $J = 2.0$ K	[47(b)]

[a] The C–M–C angles in the $[M(CN)_8]^{3-/4-}$ moiety.

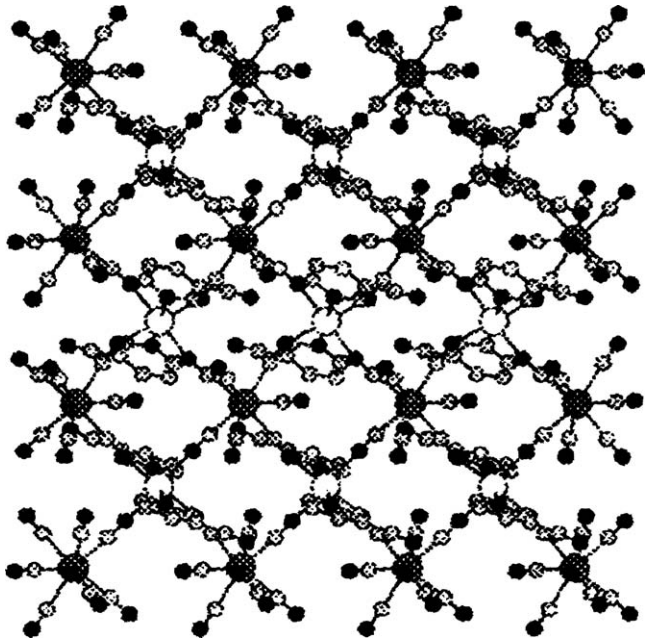

Fig. 13. Crystal structure of $Cs[Mn^{II}(3\text{-}CNpy)_2\{W^{V}(CN)_8\}]\cdot H_2O$ (hydrogen atoms, counterions and water of crystallization omitted for clarity). Reprinted with permission from Ref. [48]. Copyright 2002 The Chemical Society of Japan.

73° and 143°. The topology of the chain is mainly controlled by the stereochemistry of the cationic building blocks. Generally, the topologies of alternating zigzag and 3,2-chains are observed for Mn(II), Ni(II) and Ln(III) centres. Copper(II) complexes exhibit more sophisticated ladder, necklace and ribbon patterns. The formation of CN bridges by $[M(CN)_8]^{n-}$ entities as well as by the M′ sites is limited to 3. The mean value of the M′–N–C angle of 158.6° is similar to that found for 0D assemblies with blocking ligands at the M′ sites (160.0°). However, the average M′–N bond length of 2.30 Å is greater than that for 0D systems of 2.14 Å. The exceptional group of compounds constituted by the lanthanide-based 1D assemblies is characterized by almost linear (average of 172.3°) and exceptionally long (average of 2.56 Å) cyano-bridges. The Mn(II)–Mo(V) centres in the 3,2-chains exhibit antiferromagnetic coupling, whereas an analogous chain of Co(II)–W(V) shows ferromagnetic behaviour.

5. 2D bimetallic assemblies

A number of bimetallic octacyanometallate-based layered compounds have been recently synthesised and proven to possess interesting magnetic properties.

$Cs[Mn^{II}(3\text{-}CNpy)_2\{W^{V}(CN)_8\}]\cdot H_2O$ forms a two-dimensional folded layer structure [48]. Anionic layers are stabilised in the crystal structure by the presence of Cs^+ cations and contacts between 3-CNpy ligands from neighbouring layers (Fig. 13). The compound is a ferrimagnet with high ordering temperature of 35 K. The saturation value of magnetization of $4.1\mu_B$, results from an antiferromagnetic interaction between Mn^{II} and W^{V} within the layer, together with interlayer ferromagnetic coupling (Fig. 14). In order to explain the nature of superexchange interactions, DV-Xα calculations were performed. The results

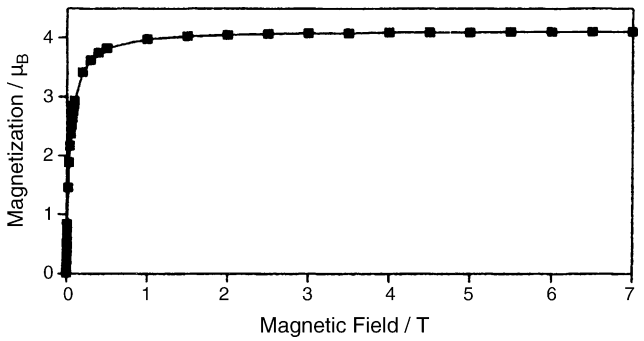

Fig. 14. Magnetization vs. external magnetic field at 5 K for $Cs[Mn^{II}(3\text{-}CNpy)_2\{W^V(CN)_8\}]\cdot H_2O$. Reprinted with permission from Ref. [48]. Copyright 2002 The Chemical Society of Japan.

indicate that overlapping of magnetic orbitals: A_1 (d_{z^2}) for W^V and A_{2g} (d_{xy} in the local symmetry) for Mn^{II} occurring through cyano bridges leads to antiferromagnetism. The ferromagnetic properties of the system may originate from dipole–dipole interactions between layers.

The self-assembly of octacyanotungstate(V), Cu^{2+} and cyanopyridine results in the formation of a two-dimensional structure [49]. Regardless of the ligand used, 3-CNpy or 4-CNpy, two similar layered structures are formed. The main difference between them is the interlayer distance, which has a significant influence on magnetic properties. $[\{Cu^{II}(3\text{-}CNpy)_2(H_2O)\}_2\{Cu^{II}(3\text{-}CNpy)_2(H_2O)_2\}\{W^V(CN)_8\}_2]$ is a metamagnet. Magnetization versus field measurements show a spin-flop transition with a critical magnetic field of 220 G. Saturation value of $5.2\mu_B$ is close to the value of $5.0\mu_B$ expected for the set of five $S = 1/2$ spins coupled ferromagnetically. FCM measurements indicate the Neel temperature of 8 K.

The second compound, $[\{Cu^{II}(4\text{-}CNpy)_2\}_2\{Cu^{II}(4\text{-}CNpy)_2(H_2O)_2\}\{W^V(CN)_8\}_2]\cdot 6H_2O$ also exhibits metamagnetism with $T_N = 4.4$ K and a critical field of 3200 G. The decrease of transition temperature can be attributed to the lengthening of the superexchange pathway between metal centres. The very large value of the critical field in comparison to the previous compound originates from the π–π stacking between cyanopyridine ligands.

Coordination networks based on octacyanometallates and nickel ions are rare. An example is $\{[Ni^{II}(pn)_2]_2[Mo^{IV}(CN)_8]\cdot 4H_2O\}_n$, which exhibits a 2D structure with a honeycomb motif [35]. The compound behaves like a paramagnet with $C = 2.40$ emu K mol^{-1}, which indicates the presence of two Ni(II) spins. The presence of weak antiferromagnetic coupling is visible both in the $\chi_M T$ plot as a dramatic decrease of signal below 20 K and also in the negative value of Weiss constant of −2.5 K.

The two-dimensional structure of $[Cu^{II}(cyclam)]_2[Mo^{IV}(CN)_8]\cdot 10.5H_2O$ reveals the topology of a square grid pattern with diamagnetic octacyanomolybdate(IV) ions placed in the nodes [50]. The thermal dependence of $\chi_M T$ is almost linear and fits the Curie–Weiss law with $C = 0.754$ emu K mol^{-1} and Weiss constant −0.3 K. Judging by the molecular structure of the assembly, it can be attributed to the presence of two Cu centres with spins $S = 1/2$ and $g = 2.01(5)$ each. The small value of the Weiss constant indicates a weak antiferromagnetic coupling through the diamagnetic Mo^{IV} metal centre.

Two structurally related coordination networks based on octacyanotungstate and copper(II) complexes with diamine ligands: $[Cu^{II}(tn)]_3[W^V(CN)_8]_2\cdot 3H_2O$ and $[Cu^{II}(pn)]_3[W^V(CN)_8]_2\cdot 3H_2O$ form 2D layered structures [51]. Both compounds show metamagnetic properties. The product of magnetic susceptibility and temperature for $[Cu^{II}(tn)]_3[W^V(CN)_8]_2\cdot 3H_2O$ shows

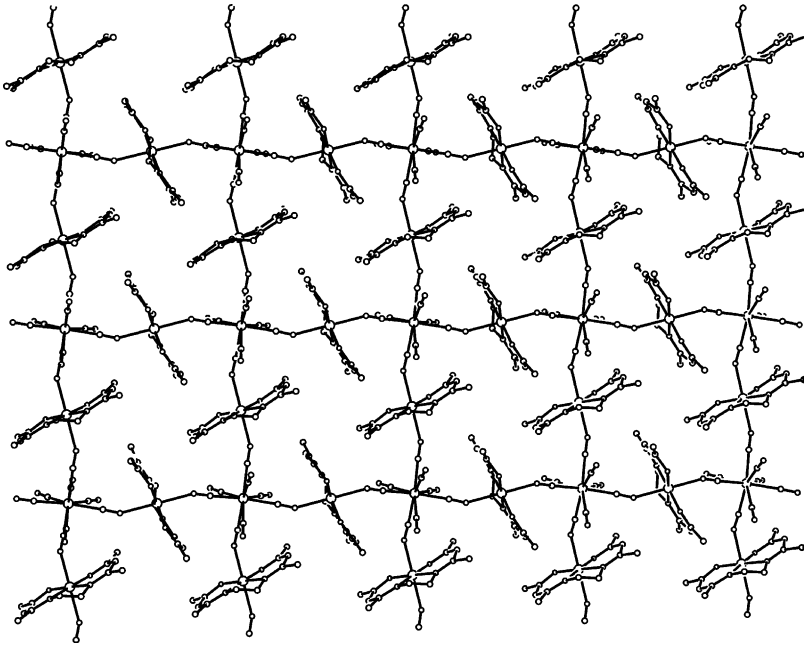

Fig. 15. Two-dimensional layer of $K[Mn^{III}(acacen)]_2[W^V(CN)_8]\cdot 2H_2O$ (hydrogen atoms, counterions and water of crystallization omitted for clarity). Reprinted with permission from Ref. [52]. Copyright 2004 Elsevier B.V.

a sharp maximum of 6.56 emu K mol^{-1} near 10 K. The magnetic susceptibility of the compound fits the Curie–Weiss law with $\theta = 19.52$ K. Ferromagnetic ordering occurs between the adjacent metal centres within the layer, while neighbouring layers interact antiferromagnetically. AC measurements reveal a frequency-independent peak of $\chi'_M T$ at 10.7 K, which is attributed to the transition from ferromagnetic to antiferromagnetic state. The sigmoidal shape of magnetization versus field curve also indicates the metamagnetic behaviour of the compound. The critical field value was found to be 1.25 T at 1.8 K. The magnetic properties of $[Cu^{II}(pn)]_3[W^V(CN)_8]_2{\cdot}3H_2O$ are similar to those of the previous assembly. It exhibits a frequency-independent $\chi'_M T$ peak at 8.1 K, indicative of long-range antiferromagnetic ordering. Magnetization studies performed at 1.8 K reveal the presence of narrow hysteresis. The spin-flip transition from antiferromagnetic to ferromagnetic state occurs at the critical field of 0.35 T.

$K[Mn^{III}(acacen)]_2[W^V(CN)_8]{\cdot}2H_2O$ forms a 2D coordination network. The structure of the assembly shows the topology of a square grid built of Mn_4W_4 octagons (Fig. 15) [52]. The measurements of magnetic susceptibility show the maximum of $\chi_M T$ value 24.7 emu K mol^{-1} at 14 K. The compound obeys the Curie–Weiss law with $\theta = 19.7$ K. The ferromagnetic ordering between Mn and W centres becomes dominating below $T_C = 18$ K. The value of the transition temperature was found from the extremum of dM/dT derivative of FCM and ZFCM curves (Fig. 16).

The two-dimensional coordination network of $[Cu^{II}(tn)_2]_2[W^V(CN)_8](OH){\cdot}H_2O$ exhibits a layered structure built of trinuclear Cu_2W units connected through long cyano bridges in the axial positions of elongated copper octahedra [53]. The magnetic properties of the compound reveal weak ferromagnetic coupling between neighbouring Cu and W

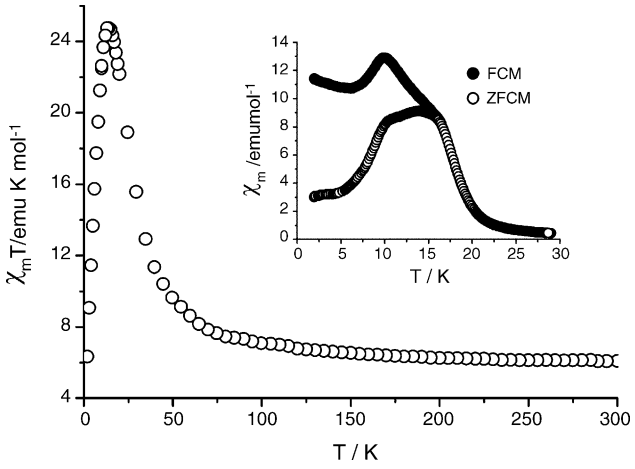

Fig. 16. Temperature dependence of $\chi_M T$ for $K[Mn^{III}(acacen)]_2[W^V(CN)_8]{\cdot}2H_2O$ measured at 10 kOe. Inset: FCM and ZFCM in an applied field of 200 Oe. Reprinted with permission from Ref. [52]. Copyright 2004 Elsevier B.V.

atoms, characterised by $\theta = 8.1$ K. The trimeric units interact antiferromagnetically at low temperature, which is pronounced by decreasing $\chi_M T$ value below 30 K. Magnetization saturation measured at 1.8 K of 2.61μ_B is smaller than the value expected for the set of two non-interacting Cu^{II} and one W^V ions (3.0μ_B).

Similar structure and magnetic properties were reported in the case of $\{[Cu^{II}(dien)]_2[W^V(CN)_8](OH){\cdot}3H_2O\}_\infty$ [53]. The structure of the assembly presents a 2D coordination network built of 24-atom macrocyclic units $W_4Cu_4(CN)_8$. Magnetic studies reveal the presence of weak ferromagnetic coupling within the layer ($\theta = 3.7$ K) and weak antiferromagnetic interlayer interaction. Despite strict orthogonality of the magnetic orbitals of Cu and W, the ferromagnetic interaction present in

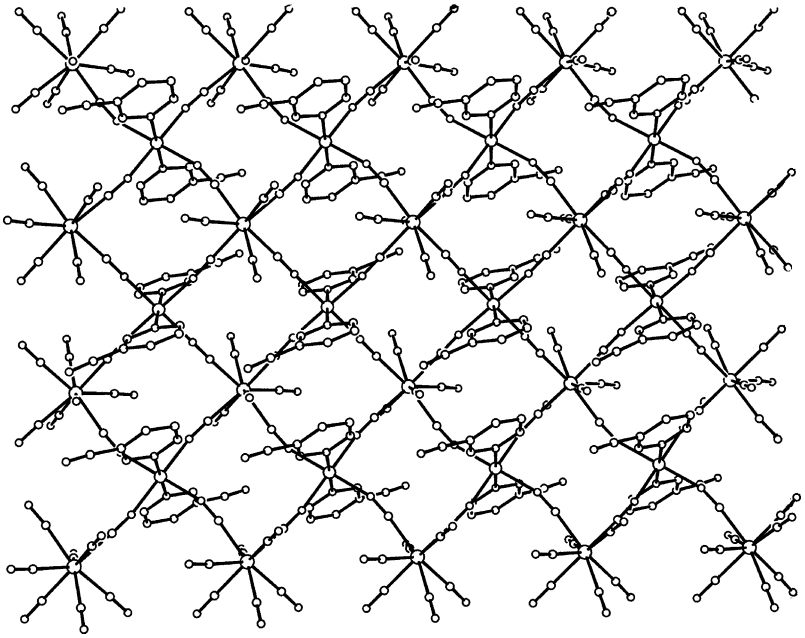

Fig. 17. A view perpendicular to the 2D layer of $Cs[\{Co^{II}(3\text{-}CNpy)_2\}\{W(CN)_8\}]{\cdot}H_2O$ (hydrogen atoms, counterions and water of crystallization omitted for clarity). Reprinted with permission from Ref. [54]. Copyright 2003 American Chemical Society.

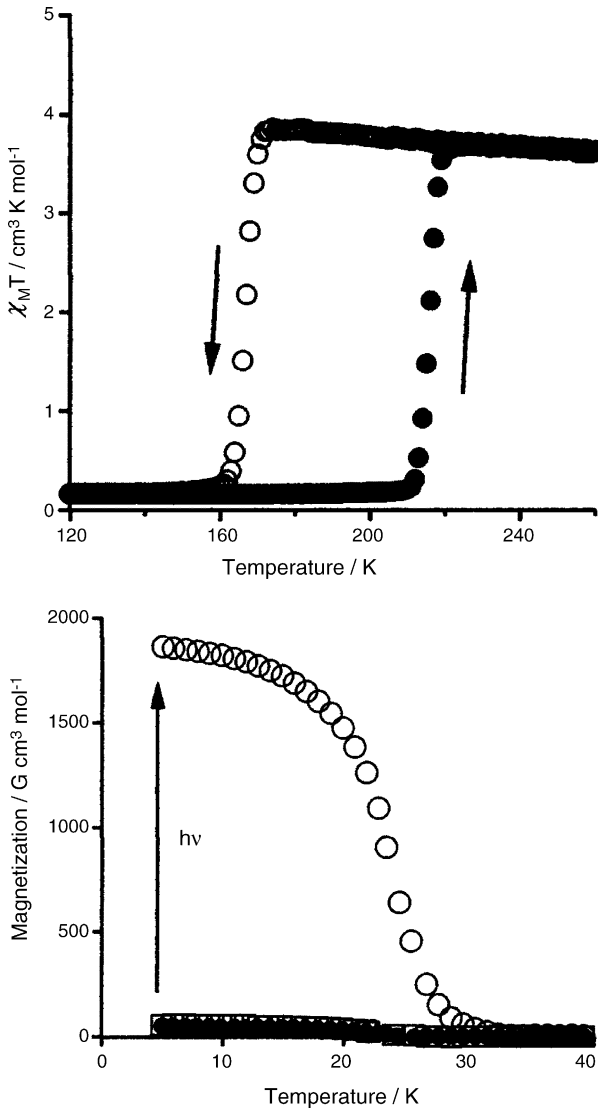

Fig. 18. (Top) Temperature dependence of $\chi_M T$ for Cs[{Co^{II}(3-CNpy)$_2$}{W(CN)$_8$}]·H$_2$O in an external field of 5 kOe measured when cooling (◯) and warming (●). (Bottom) Field-cooled magnetization in an external magnetic field of 10 Oe before irradiation (□), after irradiation (◯), and after thermal treating (5 → 120 → 5 K) (●). Reprinted with permission from Ref. [54]. Copyright 2003 American Chemical Society.

these systems is rather weak. This fact can be explained by significant deviation from linearity of Cu–N–C bridges.

The compound Cs[{Co^{II}(3-CNpy)$_2$}{W^{V}(CN)$_8$}]·H$_2$O forms a 2D structure of a folded square grid built of tetrametallic units Co$_2$W$_2$ (Fig. 17) [54]. This assembly exhibits a temperature-induced magnetic phase transition with a wide thermal hysteresis loop from 167 K (HT → LT) to 216 K (LT → HT) as well as photomagnetic effect (Fig. 18). The high temperature phase is built of Co^{II} (LS, $S = 1/2$) and W^{V} ($S = 1/2$), whereas the low temperature phase contains Co^{III} (LS, $S = 0$) and W^{IV} ($S = 0$) metal centres. Due to presence of inter-valence charge transfer band near 800 nm, the low temperature phase undergoes reversible photochemical reaction upon irradiation with red light (600–750 nm). The photoproduct contains Co^{II} (HS, $S = 3/2$) and W^{V} ($S = 1/2$) metal centres with ferromagnetically coupled spins, and shows a Curie temperature of $T_C = 30$ K. After heating to 120 K, the magnetization of the photoproduct relaxes to the initial value.

The family of isostructural 2D coordination polymers of the formula {(tetrenH$_5$)$_{0.8}$Cu$_4^{II}$[M^{V}(CN)$_8$]$_4$·7.2H$_2$O} or {(dienH$_3$)Cu$_3^{II}$[M^{V}(CN)$_8$]$_3$·4H$_2$O} (M = Mo, W) present double-layered cyano-bridged structures (Fig. 19) [55,56]. The layers are separated by protonated amine cations and water molecules. The family consists of four compounds which exhibit long-range ferrromagnetic ordering below 28–37 K. Curie temperatures were determined by AC susceptibility measurements. The maxima of χ'_M indicate the presence of ferromagnetic transition. The imaginary part of magnetic susceptibility, χ''_M displays an irregular shape below T_C. This fact can be explained by the presence of additional long-range transitions occurring in these systems. Magnetization versus field measurements reveal saturation very close to the expected value of 2 Nβ for Cu^{II}W^{V} pair. All compounds display a magnetic hysteresis loop with the coercive fields of 225 Oe for {(dienH$_3$)Cu$_3^{II}$[W^{V}(CN)$_8$]$_3$·4H$_2$O} and 30–60 Oe for other assemblies of this group (Fig. 20). Remnant magnetization reaches 0.93 Nβ for {(dienH$_3$)Cu$_3^{II}$[W^{V}(CN)$_8$]$_3$·4H$_2$O} and presents smaller values for other members of the series, indicating soft ferromagnetic behaviour of the materials. The detailed analysis of mutual orientation of magnetic orbitals in the system gives insight into the origin of the ferromagnetic interaction. The $5d_{z^2} : 5d_{x^2-y^2}$ orbital of M^{V} overlaps with empty π^* orbital of cyano ligand, which cannot be delocalised on the magnetic orbital of copper ($3d_{x^2-y^2}$). On the other hand, there is a small antiferromagnetic contribution arising from interaction of $3d_{x^2-y^2}$ orbital of copper with occupied molecular orbitals of cyanide ligand.

[Cu^{II}(dien)]$_2$[W^{IV}(CN)$_8$]·4H$_2$O and its isomorphous Mo analogue display 2D structure of strongly folded layers [46]. The presence of diamagnetic W^{IV} centres results in paramagnetic behaviour of the material, which obeys the Curie–Weiss law with $C = 0.65(1)$ emu K mol^{-1} and $\theta = -0.20(4)$ K. A weak antiferromagnetic interaction can be seen at low temperature, where the $\chi_M T$ curve decreases abruptly.

The structure of [Cu^{II}(μ-4,4′-bpy)]$_3$[W^{V}(CN)$_8$]$_2$·6DMF·2H$_2$O is an example of a 2D network of hybrid material, which involves two types of bridging ligands between metal centres: (i) cyano ligand between Cu and W, and (ii) 4,4′-bpy ligand between copper centres [57]. The system behaves like a set of ferromagnetic pentamers Cu$_3$W$_2$ with intramolecular coupling constant $J = 35(4)$ cm^{-1}. Ferromagnetic coupling occurs due to cyano bridges, which coordinate Cu centres in equatorial positions. Pentamers interact antiferromagnetically by bridges formed by axial cyano and 4,4′-bpy ligands in the coordination sphere of copper. The overall antiferromagnetic coupling is characterised by $J' = -0.05(1)$ cm^{-1}.

[Cu^{II}(tren)]{Cu^{I}[W^{V}(CN)$_8$]}·1.5H$_2$O is a rare example of heterobimetallic coordination network, which maintains two oxidation states of copper [58]. The 2D layered structure is built of Cu^{I} and W^{V} linked by cyano bridges. Layers are modified by [Cu^{II}(tren)]$^{2+}$ units coordinated to W^{V} alternatively above and below the plane. The maximum of $\chi_M T$ near 4 K indicates a fer-

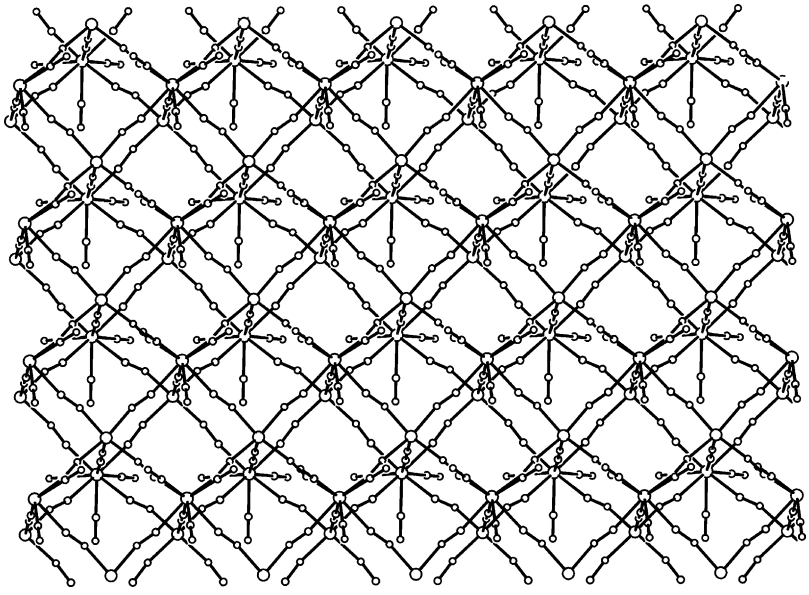

Fig. 19. The double-layered structure of $\{(tetrenH_5)_{0.8}Cu_4^{II}[M^V(CN)_8]_4\cdot 7.2H_2O\}$ and $\{(dienH_3)Cu_3^{II}[M^V(CN)_8]_3\cdot 4H_2O\}$ (M = Mo, W). Reprinted with permission from Ref. [56]. Copyright 2003 Elsevier B.V.

romagnetic transition. Fit of the Curie–Weiss law gives values of $C = 0.97$ emu K mol^{-1} and $\theta = 1.91$ K. The values of coupling constants $J_1 = 5.8(1)$ cm^{-1} and $J_2 = -0.03(1)$ cm^{-1} indicate the presence of ferromagnetic coupling within Cu^{II} and W^V pair and antiferromagnetic interaction of the dimers through diamagnetic Cu^I spacers.

The first example of 2D lanthanide- and octacyano-based system is represented by the $[Sm^{III}(H_2O)_5][W^V(CN)_8]$ assembly [59]. The X-ray structural studies revealed the grid-like pattern of the coordination network. The magnetic measurements show the cool-rate dependent ferromagnetism.

Selected geometric parameters and a summary of the magnetic properties for 2D octacyano-based systems are presented in Table 3. The 2D architectures exhibit two different motifs that organise $[M(CN)_8]^{n-}$ and M′ centres with blocking ligands into infinite two-dimensional grids. In the first type of topologies two *cis*-M′ and two M centres are placed in the opposite corners of a square with M atoms forming two additional CN bridges to extend the network. Square-grid coordination networks comprising $[M(CN)_8]^{n-}$ nodes with *cis*- or *trans*-M′ complexes located at the edges form the second type of 2D systems. One exception is $K_2\{[Co^{III}(tren)]_2[W^{IV}(CN)_8]_2\}\cdot 9H_2O$ supramolecular system which is constructed with $\{[Co^{III}(tren)]_2[W^{IV}(CN)_8]_2\}^{2-}$ squares linked by the K^+ ions coordinating cyano ligands [73]. The 2D coordination network in hybrid $[Cu^{II}(\mu\text{-}4,4'\text{-bpy})(DMF)_2][Cu^{II}(\mu\text{-}4,4'\text{-bpy})(DMF)]_2[W^V(CN)_8]_2\cdot 2DMF\cdot 2H_2O$ is built of $\{[Cu^{II}(\mu\text{-}4,4'\text{-bpy})]^{2+}\}_n$ chains cross-linked by octacyanotungstate(V) units. In two Cu(II)-based systems $(dienH_3)\{Cu_3^{II}[M^V(CN)_8]_3\}\cdot 4H_2O$ and $(tetrenH_5)_{0.8}\{Cu_4^{II}[M^V(CN)_8]_4\}\cdot 7.2H_2O$ all coordination sites at the Cu(II) centres arranged in square pyramidal geometry are occupied by the cyano bridges causing the formation of the double-layered structure.

The average M′–N–C angle of 161.6° is comparable with that found for 1D assemblies (158.6°), however the mean value of the M′–N bond length (2.13 Å) is significantly shorter than that for 1D systems (2.30 Å). In Cu(II)-based 2D coordination networks the cyano bridges are arranged into axial and equatorial positions in square pyramidal or trigonal bipyramidal geometries of Cu(II) centres. The axial coordination of longer CN bridges seems to give rise to the dominant ferromagnetic exchange between Cu(II) and M(V) paramagnetic centres.

6. 3D bimetallic assemblies

Three-dimensional (3D) octacyano-based coordination networks are the direct Prussian blue analogues. The 3D materials are attracting considerable interest from the viewpoint of the construction and their potential application as spin carriers in molecular spintronics.

The first group of 3D extended assemblies are systems based on paramagnetic $[M^V(CN)_8]^{3-}$ anionic precursors: $[Mn_2^{II}(H_2O)_2(CH_3COO)][W^V(CN)_8]\cdot 2H_2O$ [60], $Cs_{0.5}Mn_2^{II}[W^V(CN)_8](CH_3CO_2)_{1.5}\cdot H_2O$ [60], $[Mn_6^{II}(H_2O)_9][W^V(CN)_8]_4\cdot 13H_2O$ [61], $[Mn^{II}(H_2O)_2]_2[W^V(CN)_8](OH)\cdot 2H_2O$ [62], high T_C ferrimagnet $[Mn^{II}(pym)(H_2O)]_2[Mn^{II}(H_2O)_2][W^V(CN)_8]_2\cdot(pym)_2\cdot 2H_2O$ [63], $[Co^{II}(H_2O)_2]_3[W^V(CN)_8]_2\cdot 4H_2O$ built by Co(II) aqua-ion ferromagnet with $T_C = 18$ K [64], and Cu(II) complexes $[Cu_2^{II}(H_2Tea)_2]_5[W^V(CN)_8]_2[W^{IV}(CN)_8]\cdot xH_2O$ [65] and $[Cu^{II}(en)_2]_3[W^V(CN)_8]_2\cdot H_2O$ [66].

The ferrimagnetic $[Mn^{II}(pym)(H_2O)]_2[Mn^{II}(H_2O)_2][W^V(CN)_8]_2\cdot(pym)_2\cdot 2H_2O$ with $T_C = 47$ K was obtained from aqueous solution with pyrimidine as a blocking ligand [63]. The $[Mn(pym)(H_2O)]^{2+}$ and $[W(CN)_8]^{3-}$ moieties are arranged into 2D layers bound by the $[Mn(H_2O)_2]^{2+}$ pillar to form the 3D framework with 1D channels occupied by the non-coordinated

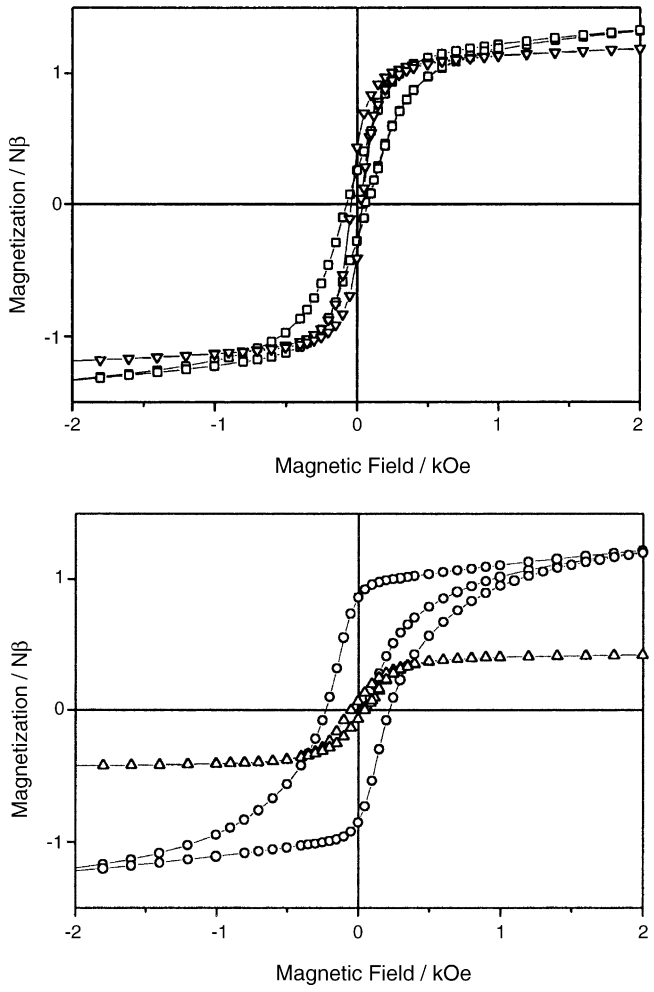

Fig. 20. Magnetic hysteresis loops at 4.38 K for $\{(tetrenH_5)_{0.8}Cu_4^{II}[W^V(CN)_8]_4\cdot 7.2H_2O\}$ (□), $\{(tetrenH_5)_{0.8}Cu_4^{II}[Mo^V(CN)_8]_4\cdot 7.2H_2O\}$ (▽) (top), $\{(dienH_3)Cu_3^{II}[W^V(CN)_8]_3\cdot 4H_2O\}$ (◯) and $\{(dienH_3)Cu_3^{II}[Mo^V(CN)_8]_3\cdot 4H_2O\}$ (△) (bottom). Reprinted with permission from Ref. [56]. Copyright 2003 Elsevier B.V.

pyrimidine molecules (Fig. 21). Magnetic studies show the ferrimagnetic behaviour as a result of an antiferromagnetic interaction between W(V) and Mn(II) centres (Fig. 22). The DV-Xα calculation performed for Mn(II) and W(V) moieties suggests that the interaction between d_{z^2} orbital of W(V) centre and d_{xy} (in the local symmetry) orbitals of Mn(II) centres through the cyano bridge orbitals gives rise to the antiferromagnetic superexchange pathway.

The 3D coordination networks based on diamagnetic $[M(CN)_8]^{4-}$ (M = Mo, W) building blocks have been widely explored resulting in the synthesis and characterization of such materials as $[Mn^{II}(bpym)(H_2O)]_2[M^{IV}(CN)_8]$ [67], $[Mn^{II}(H_2O)_2]_2[M^{IV}(CN)_8]\cdot 4H_2O$ [62], $[Fe^{II}(H_2O)_2]_2[M^{IV}(CN)_8]\cdot 4H_2O$ [68,69], $[Co^{II}(H_2O)_2]_2[M^{IV}(CN)_8]\cdot 4H_2O$ [64,70], $[Cu^{II}(en)_2][Cu^{II}(en)][M^{IV}(CN)_8]\cdot 4H_2O$ [71] and $Cu_2^{II}[M^{IV}(CN)_8]\cdot xH_2O$ [72].

The $Cu_2^{II}[M^{IV}(CN)_8]\cdot xH_2O$ systems probably have the 3D topology of the coordination network. Photomagnetic studies on $Cu_2^{II}[W^{IV}(CN)_8]\cdot 5H_2O$ and $Cu_2^{II}[Mo^{IV}(CN)_8]\cdot 7.5H_2O$ have been widely performed [72]. The MMCT bands corresponding to $Cu^{II}–M^{IV} \rightarrow Cu^{I}–M^{V}$ electron transfer were observed at 536 and 520 nm, respectively. Irradiation of a powder sample of $Cu_2^{II}[Mo^{IV}(CN)_8]\cdot 7.5H_2O$ at 530 nm provides the photomagnetic effect reversible on a thermal pathway (Fig. 23). However, in the case of $Cu_2^{II}[W^{IV}(CN)_8]\cdot 5H_2O$ system no photomagnetic effect was observed.

The relevant geometric parameters and magnetic properties for the 3D architectures are presented in Table 4. The 3D octacyano-based systems are preferably formed with cationic precursors of octahedral geometry and labile coordination sites. The self-assembly of 3D framework usually requires the number of CN bridges equal or greater than 6. The exceptions are $[Cu^{II}(en)_2][Cu^{II}(en)][M^{IV}(CN)_8]\cdot 4H_2O$ (M = Mo, W) and hybrid systems $[Mn^{II}(pym)(H_2O)]_2[Mn^{II}(H_2O)_2][W^V(CN)_8]_2\cdot(pym)_2\cdot 2H_2O$ and $[Cu_2^{II}(H_2Tea)_2]_5[W^V(CN)_8]_2[W^{IV}(CN)_8]\cdot xH_2O$. The average M′–N–C angle (158.8°) does not significantly differ from the mean values found for the systems of lower dimensionalities. However, the cyano bridges (mean M′–N bond length of 2.25 Å) are

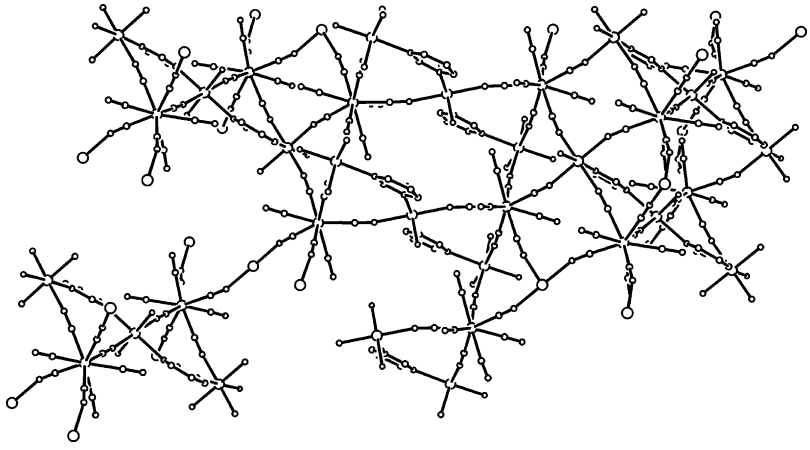

Fig. 21. The 3D framework of $[Mn^{II}(pym)(H_2O)]_2[Mn^{II}(H_2O)_2][W^V(CN)_8]_2\cdot(pym)_2\cdot 2H_2O$ (hydrogen atoms, non-coordinated pym molecules and water of crystallization omitted for clarity). Reprinted with permission from Ref. [63]. Copyright 2004 American Chemical Society.

Table 3
Relevant geometric parameters and magnetic properties for 2D bimetallic assemblies

Compound	$[M(CN)_8]^{3-/4-}$ geometry	Number of M–CN bridges	C–M–C angle (°)[a]	M′ site geometry	Number of M′–NC bridges	M′–N bond length (Å)	M′–N–C angle (°)	Magnetic properties	Reference
$Cs[Mn^{II}(3\text{-}CNpy)_2][W^V(CN)_8]\cdot H_2O$	BTP-8	4		OC-6	4			Ferrimagnetic with ordering at 35 K	[48]
$K[Mn^{III}(acacen)]_2[W^V(CN)_8]\cdot 2H_2O$	DD-8[b]	4	148.2(9)	OC-6	2	2.335(12)	151.3(14)	F with ordering at 18.9 K	[52]
$Cs[\{Co^{II}(3\text{-}CNpy)_2\}\{W^V(CN)_8\}]\cdot H_2O$	BTP-8	4	77.8(2)	OC-6	4	2.093(5)	171.3(5)	Temperature-induced phase transition	[54]
			81.7(2)			2.127	161.96		
			145.4(2)	OC-6	4	2.110(5)	172.8(6)		
			144.3(2)			2.075	174.68		
			83.8(2)						
			97.5(2)						
$K_2\{[Co^{III}(tren)]_2[W^{IV}(CN)_8]_2\}\cdot 9H_2O$	SAPR-8	2	72.9(5)	OC-6	2	1.896(12)	166.4(11)	No magnetic measurements	[73]
						1.919(12)	173.3(12)		
	SAPR-8	2	73.3(5)	OC-6	2	1.905(10)	169.9(12)		
						1.904(11)	170.7(10)		
$\{[Ni^{II}(pn)_2]_2[Mo^{IV}(CN)_8]\cdot 4H_2O\}_n$	SAPR-8[b]	4	145.72(17)	OC-6	2	2.125(4)	150.5(4)	Very weak AF	[35]
			76.11(17)			2.164(4)	145.7(4)		
				OC-6	2	2.101(4)	168.0(4)		
						2.111(4)	162.6(4)		
	SAPR-8[b]	4	74.53(17)	OC-6	2	2.157(4)	146.6(4)		
			146.01(17)			2.128(4)	150.7(4)		
				OC-6	2	2.113(4)	162.5(4)		
						2.090(4)	168.5(4)		
$[\{Cu^{II}(3\text{-}CNpy)_2(H_2O)\}_2\{Cu^{II}(3\text{-}CNpy)_2(H_2O)_2\}\{W^V(CN)_8\}_2]$	BTP-8	4	148.17(4)	OC-6	2	1.982(4)	175.8(4)	F (metamagnetism with $T_N = 8.0$ K)	[49]
			138.81(14)	OC-6	3	1.969(3)	174.8(4)		
						2.247(3)	153.46		
						1.994(3)	157.81		
$[\{Cu^{II}(4\text{-}CNpy)_2(H_2O)\}_2\{Cu^{II}(4\text{-}CNpy)_2(H_2O)_2\}\{W^V(CN)_8\}_2]\cdot 6H_2O$	BTP-8	4	138.20(17)	OC-6	2	2.489(4)	162.9(4)	AF (metamagnetism with $T_N = 4.4$ K)	[49]
			124.61(17)			2.489(4)	162.9(4)		
			74.45(17)	TBPY-5	3	1.984(4)eq	173.5(4)		
						1.976(4)eq	174.63		
						2.164(4)eq	172.20		

$[Cu^{II}(cyclam)]_2[Mo^{IV}(CN)_8]\cdot 10.5H_2O$	SAPR-8 and BTP-8 intermediate	4	72.3(6)	OC-6	2	2.517	132.16	Very weak AF	[50]
			134.2(6)			2.485	138.03		
			72.8(5)	OC-6	2	2.423	144.63		
			134.7(6)			2.496	141.54		
$[Cu^{II}(tn)]_3[W^{V}(CN)_8]_2\cdot 3H_2O$	SAPR-8	4		SPY-5	3	2.238(5)ax	152.6(5)	F layers with long-range AF ordering and metamagnetism below $T_N = 10.7$ K	[51]
						2.010(6)eq	167.3(6)		
	SAPR-8	4				1.999(6)eq	169.0(6)		
				SPY-5	3	2.003(6)eq	177.5(6)		
						2.222(5)ax	151.1(5)		
						1.998(5)eq	162.5(6)		
				SP-4	2	2.020(6)	174.7(7)		
						2.014(6)	174.5(7)		
$[Cu^{II}(pn)_3][W^{V}(CN)_8]_2\cdot 3H_2O$	SAPR-8	4		SPY-5	3	2.000(8)eq	177.2(8)	F layers with long-range AF ordering and metamagnetism below $T_N = 8.1$ K	[51]
						1.997(7)eq	156.5(7)		
	SAPR-8	4				2.372(7)ax	148.6(6)		
				SPY-5	3	2.006(7)eq	168.7(8)		
						2.291(7)ax	157.2(7)		
						1.956(7)eq	175.6(7)		
				SP-4	2	1.984(7)	169.4(7)		
						1.984(7)	166.7(8)		
$[Cu^{II}(tn)_2]_2[W^{V}(CN)_8](OH)\cdot H_2O$	SAPR-8	4	78.3(2)	OC-6	2	2.421(6)	141.8(5)	F coupling with $J = 3.57\ cm^{-1}$ and $J' = -0.14\ cm^{-1}$	[53]
			114.6(2)			3.102(7)	126.66		
			141.6(2)						
			142.2(4)						
$\{[Cu^{II}(dien)]_2[W^{V}(CN)_8](OH)\cdot 3H_2O\}_\infty$	SAPR-8	4	75.9(5)	SPY-5	2	1.959(8)ax	160.8(9)	F	[53]
			76.4(3)			2.313(8)ax	140.8(7)		
			73.4(3)						
			141.3(5)						

Table 3 (*Continued*)

Compound	$[M(CN)_8]^{3-/4-}$ geometry	Number of M–CN bridges	C–M–C angle (°)[a]	M′ site geometry	Number of M′–NC bridges	M′–N bond length (Å)	M′–N–C angle (°)	Magnetic properties	Reference
$(dienH_3)\{Cu_3^{II}[W^V(CN)_8]_3\}\cdot 4H_2O$	BTP-8	5	73.9(7)	SPY-5	5	2.135(7)ax	177(3)	F with $T_C = 37$ K (28 K for molybdate analogue)	[56]
			73.2(8)			2.005(13)eq	169.7(15)		
			81.8(4)			2.005(13)eq	169.7(15)		
						1.927(15)eq	162.5(16)		
						1.927(15)eq	162.5(16)		
$(tetrenH_5)\{Cu_5^{II}[W^V(CN)_8]_5\}\cdot 9H_2O$	BTP-8	5	74.8(5)	SPY-5	5	2.119(7)ax	177(2)	F with $T_C = 34$ K (33 K for molybdate analogue)	[55,56]
			72.3(6)			1.990(7)eq	169.8(7)		
			81.8(3)			1.990(7)eq	169.8(7)		
						1.969(7)eq	169.0(7)		
						1.969(7)eq	169.0(3)		
$[Cu^{II}(dien)]_2[W^{IV}(CN)_8]\cdot 4H_2O$	SAPR-8	4	142.00(16)	SPY-5	2	2.290(3)ax	140.7(2)	Paramagnetic	[46]
			73.48(12)			1.947(3)eq	161.5(3)		
			77.57(17)						
$[Cu^{II}(dien)]_2[Mo^{IV}(CN)_8]\cdot 4H_2O$	SAPR-8	4	142.10(12)	SPY-5	2	2.291(2)ax	140.7(2)	Paramagnetic	[46]
			73.57(9)			1.949(2)eq	161.5(3)		
			77.00(9)						
			77.13(13)						
$[Cu^{II}(\mu\text{-}4,4'\text{-bpy})(DMF)_2][Cu^{II}(\mu\text{-}4,4'\text{-bpy})(DMF)]_2[W^V(CN)_8]_2\cdot 2DMF\cdot 2H_2O$	SAPR-8	3	122.9(2)	OC-6	2	2.007(5)	151.1(6)	F	[57]
			141.1(2)			2.007(5)	151.1(6)		
			77.6(2)	SPY-5	2	2.297(5)ax	174.3(5)		
						1.992(5)eq	177.9(5)		
$[Cu^{II}(tren)]\{Cu^I[W^V(CN)_8]\}\cdot 1.5H_2O$	SAPR-8	5	97.6(2)	T-4	4	1.960(5)	170.3(5)	F	[58]
			83.31(19)			1.970(5)	158.5(5)		
			144.0(2)			1.975(5)	165.8(6)		
			75.6(2)			1.989(5)	173.2(5)		
			72.5(2)	TBPY-5	1	1.956(8)ax	161.7(6)		
			73.6(2)						
$[Sm^{III}(H_2O)_5][W^V(CN)_8]$	SAPR-8	4	144.12	MSAPR-9	4	2.534(9)	167.0(8)	Cool-rate dependent F	[59]
			79.1(4)						

[a] The C–M–C angles in the $[M(CN)_8]^{3-/4-}$ moiety.
[b] Geometry determined using the program SHAPE [41].

Table 4
Relevant geometric parameters and magnetic properties for 3D bimetallic assemblies

Compound	$[M(CN)_8]^{3-/4-}$ geometry	Number of M–CN bridges	C–M–C angle (°)[a]	M′ site geometry	Number of M′–NC bridges	M′–N bond length (Å)	M′–N–C angle (°)	Magnetic properties	Reference
$[Mn^{II}(H_2O)_2]_2[Mo^{IV}(CN)_8]\cdot 4H_2O$	SAPR-8	8	72.71(10) 78.2(2) 113.9(2) 142.2(2)	OC-6	4	2.206(4)	162.7(4)	Very weak AF	[62]
$[Mn_2^{II}(H_2O)_2(CH_3COO)][W^{V}(CN)_8]\cdot 2H_2O$	SAPR-8	8		OC-6	4	2.248(2)	165.4(2)	Ferrimagnetic	[60]
$Cs_{0.5}Mn_2^{II}[W^{V}(CN)_8](CH_3CO_2)_{1.5}\cdot H_2O$	SAPR-4	8	73.9(2) 113.2(2) 72.0(2) 73.8(2) 116.1(2) 72.5(2) 81(2) 71.1(2)(92.5(2) 133.3(2) 69.8(2) 74.5(2)	OC-6 OC-6	4 4		161.8(6) 173.9 171.3(6) 169.5 157.4(5) 168.3 163.4 165.9	Ferrimagnetic	[60]
$\{[Mn_6^{II}(H_2O)_9][W^{V}(CN)_8]_4\cdot 13H_2O\}_n$	DD-8	6	128.6(4) 94.9(4) 73.0(4) 146.0(4) 133.4(4) 78.9(4)	OC-6	5	2.237(8) 2.221(8) 2.202(9) 2.192(9) 2.173(9) 2.22(1)	162.6(9) 169.7(10) 154.5(10) 165.9(9) 161.4(9) 166(1)	Ferrimagnetic	[61]
	BTP-8	7	128.7(4) 140.1(4) 73.6(4) 76.3(4) 94.0(4) 86.3(4) 115.1(4)	 OC-6	 5	2.221(9) 2.249(8) 2.257(9) 2.240(9) 2.174(8) 2.198(8) 2.241(9)	173.8(10) 154.5(8) 165.9(9) 176.2(9) 176.9(9) 167.6(9) 164.5(10)		
	BTP-8	7	73.3(4) 145.1(4) 99.0(4) 115.8(4) 82.4(4)	 OC-6	 4	2.246(9) 2.233(10) 2.243(9) 2.199(10) 2.230(10)	163.1(9) 165.0(10) 162.8(9) 169(1) 169(1)		
	BTP-8	7	73.9(4) 140.5(4) 80.4(4) 142.5(4) 104.4(4) 119.2(4) 114.8(4)	 OC-6	 4	2.226(8) 2.213(9) 2.233(10) 2.214(9) 2.207(9) 2.22(1) 2.219(8) 2.245(9) 2.206(10)	173.6(9) 165.6(9) 164(1) 165.5(9) 164(1) 178(1) 176.9(9) 159.6(10) 164.7(10)		

Table 4 (*Continued*)

Compound	$[M(CN)_8]^{3-/4-}$ geometry	Number of M–CN bridges	C–M–C angle (°)[a]	M′ site geometry	Number of M′–NC bridges	M′–N bond length (Å)	M′–N–C angle (°)	Magnetic properties	Reference
$[Mn^{II}(bpym)(H_2O)]_2[Mo^{IV}(CN)_8]$	DD-8	6	101.0(2)	OC-6	3	2.186(3)	160.3(3)	AF with $J = -1.05\,cm^{-1}$	[67]
			69.8(1)			2.196(3)	151.2(3)		
			95.7(2)			2.155(3)	166.0(3)		
			78.8(1)						
			145.6(1)						
			124.0(2)						
$[Mn^{II}(bpym)(H_2O)]_2[W^{IV}(CN)_8]$	DD-8	6	100.9(3)	OC-6	3	2.183(4)	159.9(4)	AF with $J = -1.10\,cm^{-1}$	[67]
			92.3(2)			2.194(4)	151.9(4)		
			95.7(3)			2.148(4)	154.7(4)		
			78.6(2)						
			145.3(2)						
			124.5(2)						
$[Mn_2^{II}(H_2O)_4\{W^{IV}(CN)_8\}\cdot 4H_2O]_n$	SAPR-8	8	72.84(11)	OC-6	4	2.209(4)	165.8(4)	Very weak AF	[62]
			114.2(2)			2.248(4)	154.7(4)		
			146.00(17)						
			139.07)(17)						
			76.20(17)						
			80.51(17)						
$[Mn_2^{II}(H_2O)_4\{W^{V}(CN)_8\}(OH)\cdot 2H_2O]_n$	BTP-8	8	99.2(4)	OC-6	4	2.228(11)	155.1(9)	Very weak AF	[62]
			145.4(4)			2.222(10)	155.1(9)		
			86.7(4)			2.219(10)	159.2(11)		
			79.4(4)			2.219(12)	165.7(10)		
			94.8(4)			2.185(10)	174.5(11)		
			100.3(4)			2.205(10)	150.8(10)		
			68.1(4)			2.241(10)	172.8(10)		
			132.0(4)			2.215(10)	147.4(9)		
			71.7(4)						
			126.5(4)						
$[\{Mn^{II}(pym)(H_2O)\}_2\{Mn^{II}(H_2O)_2\}\{W^{V}(CN)_8\}_2]\cdot(pym)_2\cdot 2H_2O$	BTP-8	5	77.6(2)	OC-6	4	2.245(5)	171.6(5)	Ferrimagnetic with $T_C = 47\,K$	[63]
			143.4(2)			2.224	171.02		
			80.8(2)			2.206	159.03		
			78.1(2)			2.211	159.91		
			145.7(2)	OC-6	2	2.222(5)	168.9(6)		
			105.7(2)						
			71.7(2)						
			109.5(2)						
			144.2(2)						
			85.1(2)						

$[Fe^{II}(H_2O)_2]_2[Mo^{IV}(CN)_8]\cdot 4H_2O$	SAPR-8	8	148.3(9) 138.0(8) 71.4(4) 83.9(10) 111.3(8)	OC-6	4	2.222(10) 2.114(11)	146.0(12) 158.5(13)	Weak AF	[68,69]
	SAPR-8	8	145.3(11) 139.0(12) 73.6(3) 115.7(7)						
$[\{Co^{II}(H_2O)_2\}_2Mo^{IV}(CN)_8]\cdot 4H_2O$	SAPR-8	8	72.59(6) 113.68(13) 72.77(6) 114.05(13)	OC-6	4	2.140(2) 2.105(2)	156.0(2) 166.8(2)	Very weak AF	[70]
$\{[Co^{II}(H_2O)_2]_2[W^{IV}(CN)_8]\cdot 4H_2O\}_n$	SAPR-8	8	72.62(9) 113.7(2) 147.2(1) 138.1(1) 76.0(1) 81.7(1)	OC-6	4	2.099(3) 2.134(3)	166.5(3) 155.9(3)	Paramagnetic	[64]
$\{[Co^{II}(H_2O)_2]_3[W^{V}(CN)_8]_2\cdot 4H_2O\}_n$	SAPR-8	6	74.0(2) 140.5(2) 144.0(2) 111.4(2) 78.8(2) 71.3(2) 80.6(2)	OC-6 OC-6	4 4	2.117(4) 2.113(4) 2.068(4)	165.2(4) 163.2(4) 163.1(4)	F with $T_C = 18$ K	[64]
$\{[Cu_2{}^{II}(H_2Tea)_2]_5[W^{V}(CN)_8]_2[W^{IV}(CN)_8]\cdot xH_2O\}_\infty$	DD-8 DD-8	3 4	101.36(19) 86.97 145.3(2) 99.2(2) 143.2(2)	OC-6 OC-6 OC-6 SPY-5 SPY-5	1 1 1 1 1	1.96(4) 1.977(4) 1.943(4) 1960(5)eq 2.056(5)eq	167.1(5) 179.1(5) 176.5(5) 163.9(4) 165.4(4)	AF	[65]
$\{[Cu^{II}(en)_2][Cu^{II}(en)][M^{IV}(CN)_8]\cdot 4H_2O\}_n$ (M = Mo, W)	SAPR-8	5	137.1(2) 84.00(17) 74.13(17) 121.17(16) 76.80(16) 72.81(15)	SPY-5 OC-6 OC-6	3 2 2	2.222(4) 1.992(4)eq 1.990(4)eq 2.644(5) 2.500(4)	150.1(3) 163.9(3) 158.8(4) 122.0(4) 133.9(4)	No magnetic measurements reported	[71]
$\{[Cu^{II}(en)_2]_3[W^{V}(CN)_8]_2\cdot H_2O\}_\infty$	SAPR-8	6	144.6(3) 72.0(3) 112.7(3)	OC-6 OC-6	2 2 2	2.329(6) 2.967(7) 2.534(7)	139.27 115.69 142.96	F	[66]
	SAPR-8 and BTP-8 intermediate	0	80.1(3) 78.0(3) 116.3(3) 75.0(3)	OC-6 OC-6 OC-6	2 2 2	2.616(7) 2.616(7) 2.731(6)	130.49 120.77 122.69		

[a] The C–M–C angles in the $[M(CN)_8]^{3-/4-}$ moiety.

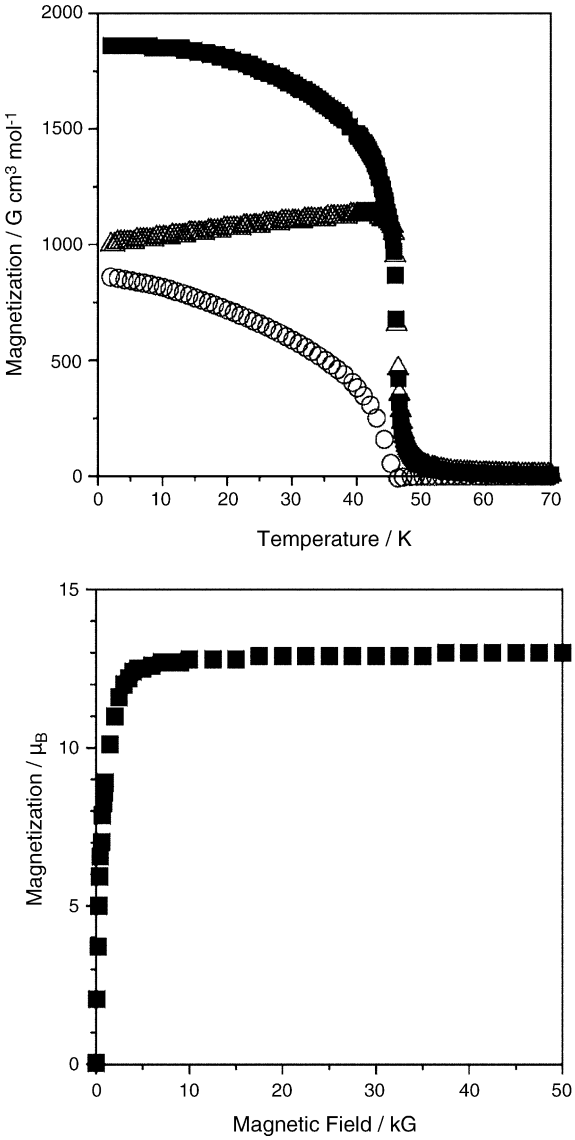

Fig. 22. (Top) The M vs. T plots for $[Mn^{II}(pym)(H_2O)]_2[Mn^{II}(H_2O)_2][W^V(CN)_8]_2\cdot(pym)_2\cdot 2H_2O$: (■) FCM for 70 → 2 K in an external magnetic field of 10 G, (△) ZFCM for 2 → 70 K in an external magnetic field of 10 G, and (◯) remanent magnetization for 2 → 70 K in an external magnetic field of 10 G. (Bottom) M vs. H measured at 2 K. Reprinted with permission from Ref. [63]. Copyright 2004 American Chemical Society.

considerably longer than M′–N links in 0D and 2D systems. Generally, the 3D coordination networks with Mn^{II}–NC–M^V bridges seem to exhibit dominant antiferromagnetic interactions between paramagnetic metal centres giving an overall ferrimagnetic effect. However, in $\{[Co^{II}(H_2O)_2]_3[W^V(CN)_8]_2\cdot 4H_2O\}_n$ and $\{[Cu^{II}(en)_2]_3[W^V(CN)_8]_2\cdot H_2O\}_\infty$ ferromagnetic coupling mediated by the Co^{II}–NC–W^V and Cu^{II}–NC–W^V bridges has been observed. Exceptionally, the hybrid 3D $\{[Cu_2^{II}(H_2Tea)_2]_5[W^V(CN)_8]_2[W^{IV}(CN)_8]\cdot xH_2O\}_\infty$ system exhibits dominant antiferromagnetic coupling attributed to the antiferromagnetic exchange interactions through the alkoxyl bridges.

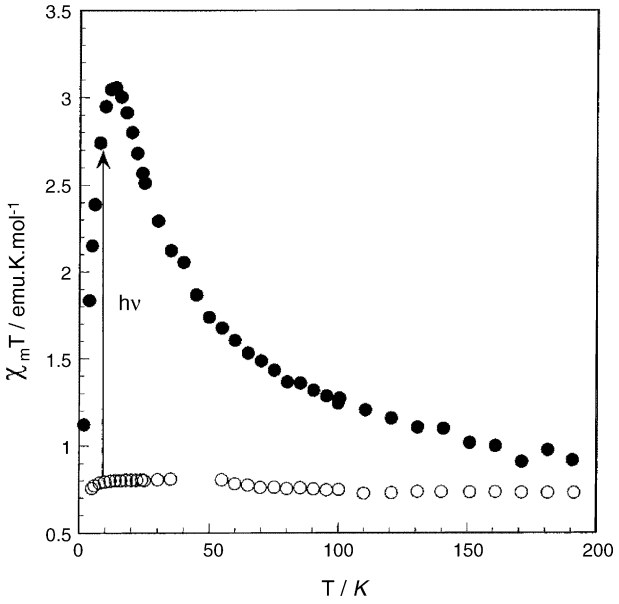

Fig. 23. $\chi_M T$ vs. T plot for $Cu_2^{II}[Mo^{IV}(CN)_8]\cdot 7.5H_2O$ before (◯) and after (●) irradiation. Reprinted with permission from Ref. [72]. Copyright 2001 American Chemical Society.

7. Conclusions and outlook

In this review we have presented the fascinating structural diversity of octacyano-based coordination networks and the complexity of their magnetic behaviour.

The octacyanometalate building block is able to generate cyano-bridged heterobimetallic systems displaying all possible dimensionalities. The prediction of the rich topology of polynuclear systems based on octacyanometalates is still a challenge. Despite this, the possible way to understand the formation of extended architectures is the preference given to certain geometries of cationic building blocks. Moreover, the topology of the polynuclear coordination network strongly depends on the group of C–M–C angles in the octacyanometalate moiety (about 75°, 115° and 142°) chosen by the cationic precursor. Essentially, the geometry and the number of the labile coordination sites at the cationic building block is the main aspect determining the choice of the C–M–C angles. However, there are more subtle effects (solvents, counterions, competition between solvent and cyano bridging in the substitution reaction, etc.) which influence the final topology.

We have shown that, generally, multidimensional polynuclear systems based on cationic Mn(II) and Mn(III) complexes are characterized by a dominant intramolecular antiferromagnetic interaction. According to recently performed theoretical calculations, the spherical symmetry of the spin density at Mn centres appears to be the rational explanation of antiferromagnetism in Mn-based coordination networks [27]. There is only one exception, the 2D $K[Mn^{III}(acacen)]_2[W^V(CN)_8]\cdot 2H_2O$ system, where ferromagnetic ordering with $T_C = 18$ K has been found.

The multidimensional assemblies derived from Cu(II) precursors usually display a ferromagnetic Cu(II)–W(V) interaction. The ferromagnetic exchange seems to be mediated through the axially coordinated cyano bridges in square pyramidal, trigonal

bipyramidal or octahedral geometries of Cu(II) centres. The antiferromagnetic interactions found in the photomagnetic $[Cu^{II}(2,2'\text{-bpy})_2]_2[Mo^{IV}(CN)_8]\cdot 5H_2O\cdot MeOH$ and 2D $[\{Cu^{II}(4\text{-CNpy})_2(H_2O)\}_2\{Cu^{II}(4\text{-CNpy})_2(H_2O)_2\}\{W^{V}(CN)_8\}_2]\cdot 6H_2O$ appear to result from the equatorial coordination of cyano bridges at the Cu(II) centres. Exceptionally, in the 3D $\{[Cu_2^{II}(H_2Tea)_2]_5[W^{V}(CN)_8]_2[W^{IV}(CN)_8]\cdot xH_2O\}_\infty$ hybrid system, antiferromagnetic exchange has been reported as a result of magnetic interactions through the alkoxyl bridges.

We have outlined the various ways leading to the realization of the multifunctionality of the octacyano-based molecular materials. The most promising assemblies from the viewpoint of potential application in modern nanotechnology are the high-spin polynuclear clusters, molecules displaying the spin reorientation phenomenon and the extended coordination networks combining the optical and magnetic properties. We can envisage further development of multinuclear complexes based on octacyanometalates leading towards spin carriers in molecular spintronics.

Acknowledgements

This work was supported by the Committee for Scientific Research in Poland (KBN) (grants nos. 3T09A 15126 and 2P03B 111 24). BS is grateful to all coworkers whose names appear in the references.

References

[1] A. Chilesotti, Gazz. Chim. Ital. 34II (1904) 493.
[2] A. Rosenheim, A. Garfunkel, F. Kohn, Z. Anorg. Allg. Chem. 65 (1910) 166.
[3] (a) O. Olsson, Berichte der Deutschen Chemischen Gesellschaft 47 (1914) 917;
(b) O. Olsson, Z. Anorg. Allg. Chem. 88 (1914) 49.
[4] O. Collenberg, Z. Anorg. Allg. Chem. 136 (1924) 245.
[5] (a) A. Samotus, J. Szklarzewicz, Coord. Chem. Rev. 125 (1993) 63;
(b) B. Sieklucka, Wiad. Chem. 47 (1993) 535;
(c) J.G. Leipoldt, S.S. Basson, A. Roodt, Adv. Inorg. Chem. 40 (1993) 241;
(d) J.G. Leipoldt, S.S. Basson, A. Roodt, W. Purcell, Polyhedron 11 (1992) 2277.
[6] M. Verdaguer, A. Bleuzen, V. Marvaud, J. Vaissermann, M. Seuleiman, C. Desplanches, A. Scuiller, C. Train, R. Garde, G. Gelly, C. Lomenech, I. Rosenman, P. Veillet, C. Cartier, F. Villain, Coord. Chem. Rev. 190–192 (1999) 1023, and references therein.
[7] B. Sieklucka, R. Podgajny, P. Przychodzeń, T. Korzeniak, Coord. Chem. Rev. 249 (2005) 2203.
[8] (a) J.G. Leipoldt, L.D.C. Bok, P.J. Cilliers, Z. Anorg. Allg. Chem. 409 (1974) 343;
(b) J.G. Leipoldt, L.D.C. Bok, P.J. Cilliers, Z. Anorg. Allg. Chem. 407 (1974) 350.
[9] L.D.C. Bok, J.G. Leipoldt, S.S. Basson, Z. Anorg. Allg. Chem. 415 (1975) 81.
[10] C.R. Dennis, A.J. van Wyk, S.S. Basson, J.G. Leipoldt, Transition Met. Chem. 17 (1992) 471.
[11] S.S. Basson, L.D.C. Bok, S.R. Grobler, Z. Anal. Chem. 268 (1974) 287.
[12] (a) B. Sieklucka, Inorg. Chim. Acta 186 (1991) 179;
(b) B. Sieklucka, A. Samotus, J. Photochem. Photobiol. A: Chem. 74 (1993) 115.
[13] (a) W.L. Waltz, A.W. Adamson, P.D. Fleishauer, J. Am. Chem. Soc. 89 (1967) 3923;
(b) W.L. Waltz, A.W. Adamson, J. Chem. Phys. 73 (1969) 4250;
(c) M. Shirom, Y. Siderer, J. Chem. Phys. 57 (1972) 1013;
(d) O. Kalisky, M. Shirom, J. Photochem. 7 (1977) 215.
[14] (a) H. Hennig, A. Rehorek, M. Ackermann, D. Rehorek, Ph. Thomas, Z. Anorg. Allg. Chem. 496 (1983) 186;
(b) H. Hennig, A. Rehorek, D. Rehorek, Ph. Thomas, Inorg. Chim. Acta 86 (1984) 41;
(c) H. Hennig, R. Benedix, R. Billing, J. Prakt. Chem. 328 (1986) 829;
(d) R. Billing, D. Rehorek, J. Salvetter, H. Hennig, Z. Anorg. Allg. Chem. 557 (1988) 234.
[15] (a) R.A. Pribush, R.D. Archer, Inorg. Chem. 13 (1974) 2556;
(b) P.M. Kiernan, Inorg. Chim. Acta 20 (1976) 89;
(c) D.L. Kepert, Inorganic Stereochemistry, Springen-Verlag, Berlin, 1982, p. 152 (Chapter 12);
(d) J.K. Burdett, R. Hoffmann, R.C. Fay, Inorg. Chem. 17 (1978) 2553.
[16] (a) M.J. Scott, R.H. Holm, J. Am. Chem. Soc. 116 (1994) 11357;
(b) M.J. Scott, S.C. Lee, R.H. Holm, Inorg. Chem. 33 (1994) 4651;
(b) M.T. Gardner, G. Deinum, Y. Kim, G.T. Babcock, M.J. Scott, R.H. Holm, Inorg. Chem. 35 (1996) 6878;
(b) B.S. Lim, R.H. Holm, Inorg. Chem. 37 (1998) 4898.
[17] P.M. Kiernan, W.P. Griffith, J. Chem. Soc. Dalton Trans. (1975) 2489.
[18] O. Kahn, Molecular Magnetism, VCH, New York, 1993, p. 150.
[19] P.J. Haÿ, J.C. Thibeault, R. Hoffmann, J. Am. Chem. Soc. 97 (1975) 4884.
[20] J.J. Girerd, Y. Journeaux, O. Kahn, Chem. Phys. Lett. 82 (1981) 534.
[21] O. Kahn, Molecular Magnetism, VCH, New York, 1993, p. 187.
[22] A. Dei, Angew. Chem. Int. Ed. 44 (2005) 1160.
[23] O. Sato, J. Photochem. Photobiol. C: Photochem. Rev. 5 (2004) 203.
[24] O. Sato, Y. Einaga, A. Fujishima, K. Hashimoto, Inorg. Chem. 38 (1999) 4405.
[25] O. Sato, Y. Einaga, T. Iyoda, A. Fujishima, K. Hashimoto, J. Electrochem. Soc. 144 (1997) L11.
[26] J. Larionova, M. Gross, M. Pilkington, H. Andres, H. Stoeckli-Evans, H. Güdel, S. Decurtins, Angew. Chem. Int. Ed. 39 (2000) 1605.
[27] E. Ruiz, G. Rajaraman, S. Alvarez, B. Gillon, J. Stride, R. Clérac, J. Larionova, S. Decurtins, Angew. Chem. Int. Ed. 44 (2005) 2711.
[28] Z.J. Zhong, H. Seino, Y. Mizobe, M. Hidai, A. Fujishima, S. Ohkoshi, K. Hashimoto, J. Am. Chem. Soc. 122 (2000) 2952.
[29] Y. Song, P. Zhang, X.-M. Ren, X.-F. Shen, Y.-Z. Li, X.-Z. You, J. Am. Chem. Soc. 127 (2005) 3708.
[30] F. Bonadio, M. Gross, H. Stoeckli-Evans, S. Decurtins, Inorg. Chem. 41 (2002) 5891.
[31] R. Pradhan, C. Desplanches, Ph. Guionneau, J.-P. Sutter, Inorg. Chem. 42 (2003) 6607.
[32] R. Podgajny, C. Desplanches, B. Sieklucka, R. Sessoli, V. Villar, C. Paulsen, W. Wernsdorfer, Y. Dromzee, M. Verdaguer, Inorg. Chem. 41 (2002) 1323.
[33] P. Przychodzeń, K. Lewiński, M. Bałanda, R. Pełka, M. Rams, T. Wasiutyński, C. Guyard-Duhayon, B. Sieklucka, Inorg. Chem. 43 (2004) 2967.
[34] H. Kou, B.Ch. Zhou, Sh. Si, R. Wang, Eur. J. Inorg. Chem. (2004) 401.
[35] F. Chang, H.-L. Sun, H.-Z. Kou, S. Gao, Inorg. Chem. Commun. 5 (2002) 660.
[36] P. Przychodzeń, M. Rams, C. Guyard-Duhayon, B. Sieklucka, Inorg. Chem. Commun. 8 (2005) 350.
[37] B. Sieklucka, J. Szklarzewicz, T.J. Kemp, W. Errington, Inorg. Chem. 39 (2000) 5156.
[38] C. Mathonière, R. Podgajny, Ph. Guionneau, Ch. Labrugere, B. Sieklucka, Chem. Mater. 17 (2005) 442.
[39] G. Rombaut, M. Verelst, S. Golhen, L. Ouahab, C. Mathonière, O. Kahn, Inorg. Chem. 40 (2001) 1151.
[40] J.M. Herrera, V. Marvaud, M. Verdaguer, J. Marrot, M. Kalisz, C. Mathonière, Angew. Chem. Int. Ed. 43 (2004) 5468.
[41] M. Llunell, D. Casanova, J. Cirera, J.M. Bofill, P. Alemany, S. Alvarez, M. Pinsky, D. Avnir, SHAPE v1.1b. Program for the Calculation of Continuous Shape Measures of Polygonal and Polyhedral Molecular Fragments, University of Barcelona, Spain, 2005.

[42] G. Rombaut, S. Golhen, L. Ouahab, C. Mathonière, O. Kahn, J. Chem. Soc. Dalton Trans. (2000) 3609.
[43] D. Li, S. Gao, L. Zheng, W. Tang, J. Chem. Soc. Dalton Trans. (2002) 2805.
[44] D. Li, L. Zheng, Y. Zhang, J. Huang, S. Gao, W. Tang, Inorg. Chem. 42 (2003) 6123.
[45] Y.S. You, D. Kim, Y. Do, S.J. Oh, C.S. Hong, Inorg. Chem. 43 (2004) 6899.
[46] R. Podgajny, T. Korzeniak, K. Stadnicka, Y. Dromzee, N.W. Alcock, W. Errington, K. Kruczała, M. Bałanda, T.J. Kemp, M. Verdaguer, B. Sieklucka, Dalton Trans. (2003) 3458.
[47] (a) S. Ikeda, T. Hozumi, K. Hashimoto, S.I. Ohkoshi, Dalton Trans. (2005) 2120;
(b) P. Przychodzeń, K. Lewiński, R. Pełka, M. Bałanda, K. Tomala, B. Sieklucka, Dalton Trans. (2006).
[48] Y. Arimoto, Sh. Ohkoshi, Zh.J. Zhong, H. Seino, Y. Mizobe, K. Hashimoto, Chem. Lett. 8 (2002) 832.
[49] Sh. Ohkoshi, Y. Arimoto, T. Hozumi, H. Seino, Y. Mizobe, K. Hashimoto, Chem. Commun. (2003) 2772.
[50] J. Larionova, R. Clérac, B. Donnadieu, St. Willemin, Ch. Guérin, Crystal Growth Design 3 (2003) 267.
[51] D. Li, L. Zheng, X. Wang, J. Huang, S. Gao, W. Tang, Chem. Mater. 15 (2003) 2094.
[52] H.Z. Kou, Z.H. Ni, B.C. Zhou, R.J. Wang, Inorg. Chem. Commun. 7 (2004) 1150.
[53] D. Li, S. Gao, L. Zheng, K. Yu, W. Tang, New. J. Chem. 26 (2002) 1190.
[54] Y. Arimoto, Sh. Ohkoshi, Z.J. Zhong, H. Seino, Y. Mizobe, K. Hashimoto, J. Am. Chem. Soc. 125 (2003) 9240.
[55] R. Podgajny, T. Korzeniak, M. Bałanda, T. Wasiutyński, W. Errington, T.J. Kemp, N.W. Alcock, B. Sieklucka, Chem. Commun. (2002) 1138.
[56] T. Korzeniak, R. Podgajny, N.W. Alcock, K. Lewiński, M. Bałanda, T. Wasiutyński, B. Sieklucka, Polyhedron 22 (2003) 2183.
[57] T. Korzeniak, K. Stadnicka, M. Rams, B. Sieklucka, Inorg. Chem. 43 (2004) 4811.
[58] T. Korzeniak, K. Stadnicka, R. Pełka, M. Bałanda, K. Tomala, K. Kowalski, B. Sieklucka, Chem. Commun. (2005) 2939.
[59] T. Hozumi, S.I. Ohkoshi, Y. Arimoto, H. Seino, Y. Mizobe, K. Hashimoto, J. Phys. Chem. B 107 (2003) 11571.
[60] Y. Song, Sh. Ohkoshi, Y. Arimoto, H. Seino, Y. Mizobe, K. Hashimoto, Inorg. Chem. 42 (2003) 1848.
[61] Z.J. Zhong, H. Seino, Y. Mizobe, M. Hidai, M. Verdaguer, S. Ohkoshi, K. Hashimoto, Inorg. Chem. 39 (2000) 5095.
[62] W. Dong, Y.Q. Sun, L.N. Zhu, D.Z. Liao, Z.H. Jiang, Sh.P. Yan, P. Cheng, New J. Chem. 27 (2003) 1760.
[63] T. Kashiwagi, S.I. Ohkoshi, H. Seino, Y. Mizobe, K. Hashimoto, J. Am. Chem. Soc. 126 (2004) 5024.
[64] J.M. Herrera, A. Bleuzen, Y. Dromzée, M. Julve, F. Lloret, M. Verdaguer, Inorg. Chem. 42 (2003) 7052.
[65] F. Chen, D. Li, S. Gao, X. Wang, Y. Li, L. Zheng, W. Tang, Dalton Trans. (2003) 3283.
[66] D. Li, S. Gao, L. Zheng, W. Sun, T. Okamura, N. Ueyama, W. Tang, New J. Chem. 26 (2002) 485.
[67] J.M. Herrera, D. Armentano, G. de Munno, F. Lloret, M. Julve, M. Verdaguer, New. J. Chem. 27 (2003) 128.
[68] A.K. Sra, G. Rombaut, F. Lahitête, S. Golhen, L. Ouahab, C. Mathonière, J.V. Yakhmi, O. Kahn, New J. Chem. 24 (2000) 871.
[69] G. Rombaut, C. Mathonière, Ph. Guionneau, St. Golhen, L. Ouahab, M. Verelst, P. Lecante, Inorg. Chim. Acta 326 (2001) 27.
[70] F. Tuna, St. Golhen, L. Ouahab, J.P. Sutter, C. R. Chimie 6 (2003) 377.
[71] D.F. Li, D.X. Yang, S.A. Li, W.X. Tang, Inorg. Chem. Commun. 5 (2002) 791.
[72] G. Rombaut, M. Verelst, S. Golhen, L. Ouahab, C. Mathonière, O. Kahn, Inorg. Chem. 40 (2001) 1151.
[73] R. Kania, K. Lewiński, B. Sieklucka, Dalton Trans. (2003) 1033.